Metabolic adaptations in proliferating cells and cancer

A DISSERTATION
SUBMITTED TO THE FACULTY OF THE GRADUATE SCHOOL
OF THE UNIVERSITY OF MINNESOTA
BY

Eric Allan Hanse

IN PARTIAL FULFILLMENT OF THE REQUIREMENTS
FOR THE DEGREE OF
DOCTOR OF PHILOSOPHY

Advisor: Ameeta Kelekar, Ph.D.

June 2017

Acknowledgements

There is not enough space here to acknowledge all the people who have contributed to this thesis. There are a few that need to be highlighted as without them, this work would not have been possible.

First, my advisor Ameeta Kelekar, who has been incredibly supportive of my career and developing my skills to be independent. She has been a fierce advocate for me and for my work and without her efforts I would not have achieved so much.

Second, my wife who has completely upended her life and career so that I may chase this fickle friend, science. She continues to take on unspeakable domestic burden to allow me to be fully engaged with my science.

Next, my kids Reece and Micah who have had to deal with a semi-absentee father for the past few years. I hope that by missing some of the critical moments during your growth, I have at least been a good example of what it takes to set and achieve goals.

Thank you to Jeff Albrecht, M.D. who has instilled immense confidence and courage in me both of which were incredibly useful in developing this project.

I'd like to thank members of the Kelekar lab specifically, Yan Yan who has been incredibly helpful with discussions and advice. I'd also like to thank Dr. Xazmin Lowman, Dr. Jenna Benson, Ryan Graff, Aditi Bapat, Michael Downey, Sean Nelson, Brian Wisnoski, Ben Wilke, Seokwon Jo and Maram Essawy who have all contributed to this project.

Thank you to our collaborators Maureen Kachman, Chunhai Ruan, Dongyu Wang at the University of Michigan for assistance with metabolomics. Thank you to Christine Henzler for invaluable help with bioinformatics. Thank you Todd Markowski and LeeAnn Higgins for help designing and executing a successful proteomics experiment.

Finally, I would like to thank my thesis committee David Bernlohr, Doug Mashek, David Masopust and Carol Lange who have all dedicated time and effort into my development and the quality of this project.

Dedication

I dedicate this thesis to my mother –
Patricia Joanne Hanse, who believed in me when I didn't believe in myself.

Abstract

The studies described in this dissertation focus on metabolic adaptations that occur during cell proliferation. In the first part of the thesis we focus on the Warburg effect which is a major hallmark of proliferating cells. We provide evidence that increased glucose consumption in proliferating cells requires malate dehydrogenase 1 (MDH1) to help regenerate the NAD required to sustain high levels of glycolysis. This NAD regeneration has previously only been attributed to lactate dehydrogenase (LDH). We found LDH was dispensable for proliferation whereas MDH1 was not. We also report the *MDH1* gene is amplified in a significant number of human tumors and correlates with poor prognosis. We go on to show glutamine, not glucose is a carbon source for MDH1 during proliferation, which allows more of the glucose carbon consumed to go toward biomass production. The second part of the thesis focuses on glutamine metabolism. The increased consumption and metabolism of glutamine leads to increased cellular concentrations of alpha-ketoglutarate (αKG) a tumor suppressor metabolite that affects gene expression via non-metabolic co-factor functions. One of these functions is the activation of the cytosine demethylase, Tet. Increased αKG concentrations therefore change the tumor cell's epigenetic landscape which can cause differentiation and growth arrest. We reasoned cancer cells must have mechanisms in place to prevent the tumor suppressor activity of αKG. We demonstrate that over-expression of the one carbon metabolism pathway which generates methyl groups and the cytosine methyl-transferase, DNMT1 provide an αKG resistance mechanism. We find combining αKG treatment with low concentrations of the DNMT1 inhibitor decitabine causes significant cell death and reveals a potential therapeutic vulnerability in glutamine addicted cancers. Taken together, our studies provide significant insight into the general biology of proliferative metabolism. Through these insights, our work opens new avenues for targeting the energy and biomass producing pathways cancer cells depend on to proliferate.

Table of Contents

List of Figures

Chapter 1: Introduction

Chapter 2: MDH1 regenerates cytosolic NAD for glycolysis in proliferating cells

Chapter 3: Cytosolic MDH1 utilizes glutamine derived carbons to support glycolysis

Chapter 4: Resistance to chronic αKG treatment

Chapter 5: Targeting one carbon metabolism in αKG resistant cells

Chapter 1
Introduction

Switching from a quiescent to a proliferative state requires a cell to significantly alter its consumption and disbursement of resources. Cellular proliferation entails controlled allocation of carbons to a variety of anabolic pathways, and cancer cells have exploited and reprogrammed these pathways to sustain prolonged proliferation. Otto Warburg had observed, nearly a century ago, that solid tumors increased their glucose consumption and lactate production(Warburg et al., 1927). These seminal observations have withstood the test of time and, although our understanding of the pathways cancer cells use to support their need to grow is much broader and deeper, even today increased glucose consumption and lactate production are universally accepted as hallmarks of proliferative metabolism. While Warburg's hypothesis could explain the rapid uptake and (albeit inefficient) metabolism of glucose as a means for meeting the energy demands of cell growth and division, it could not explain how cells were able to continue to grow and proliferate. Meanwhile, reports of proliferating cells utilizing glucose carbons for biomass production were beginning to emerge, creating a conundrum.

Once the cell cycle is initiated, several metabolic pathways are altered to prepare the cell for division (Figure 1-1). For example, the Pentose Phosphate Pathway (PPP) usurps some glucose carbon early in the glycolytic process for production of ribose-5 phosphate, the backbone for nucleotides needed for DNA synthesis. In addition, the PPP generates 2 molecules of NADPH, a key reductive molecule that protects cells from increased reactive oxygen species (ROS) and a necessary co-factor for *de novo* lipid synthesis (Lunt and Vander Heiden, 2011).
As glucose carbon progresses through glycolysis it is also diverted, as dihydroxyacetone phosphate (DHAP), to supply the cell with glycerol 3-phosphate, the phospholipid cap needed for the synthesis of cell membrane (Lunt and Vander Heiden, 2011).

Later in glycolysis, 3-phosphoglycerate is used for the synthesis of serine, glycine and cysteine which, besides serving as important amino acids and amino acid

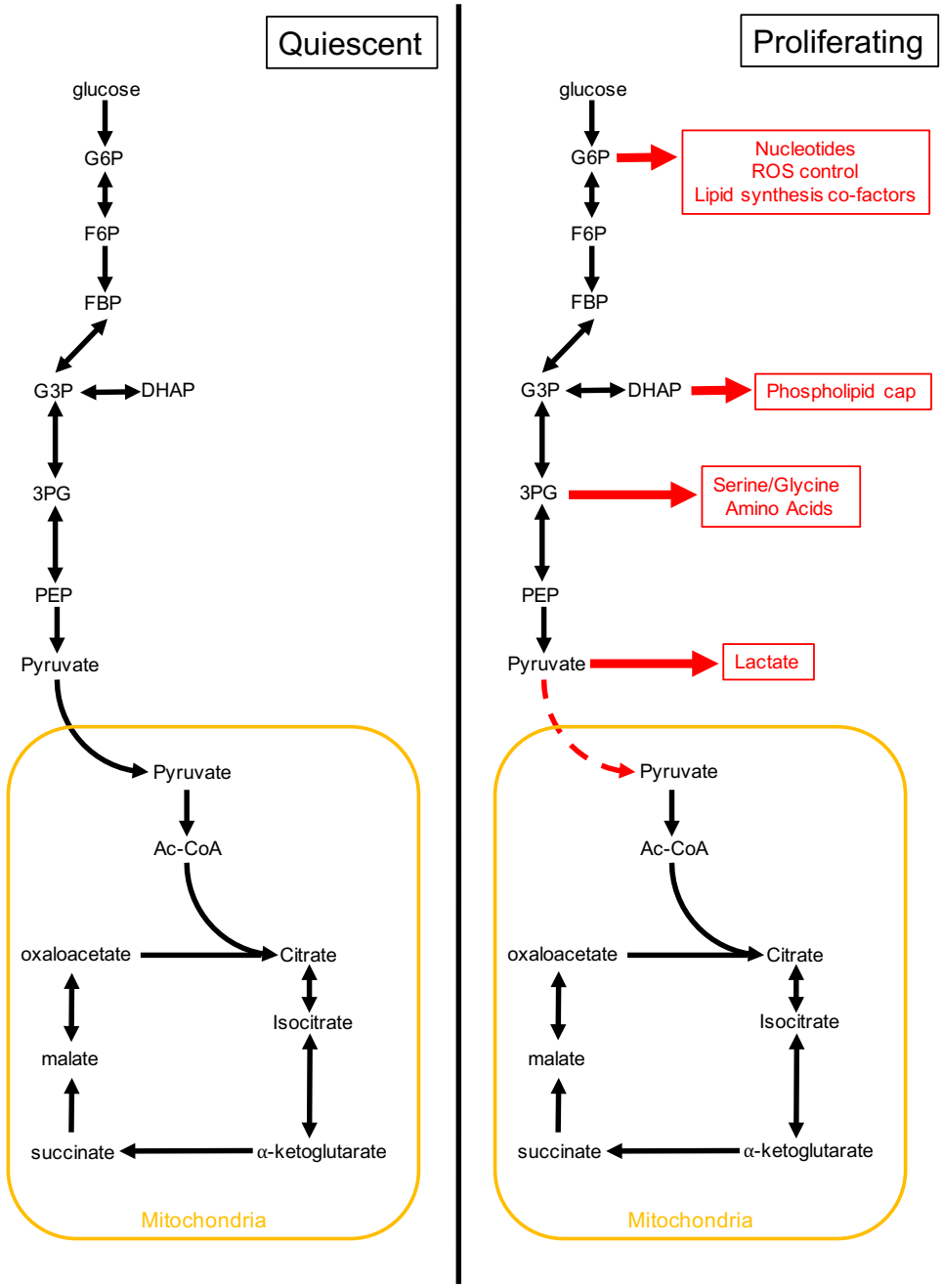

Figure 1-1. Glucose carbon handling during quiescence and proliferation. Schematic depiction of glycolysis during proliferation (left) and re-redirection of glucose carbon for biomass production and redox control during proliferation (right).

precursors, are also starting points for macromolecular synthesis through the tetrahydrofolate (THF) and ceramide (cholesterol) pathways used for membrane synthesis and nucleotides respectively (Lunt and Vander Heiden, 2011).

The Warburg Effect

The demand for biomass production during proliferation is high; therefore, it is not surprising that glucose consumption increases to meet this demand. Otto Warburg observed the increased glucose consumption in proliferating tumor cells in the

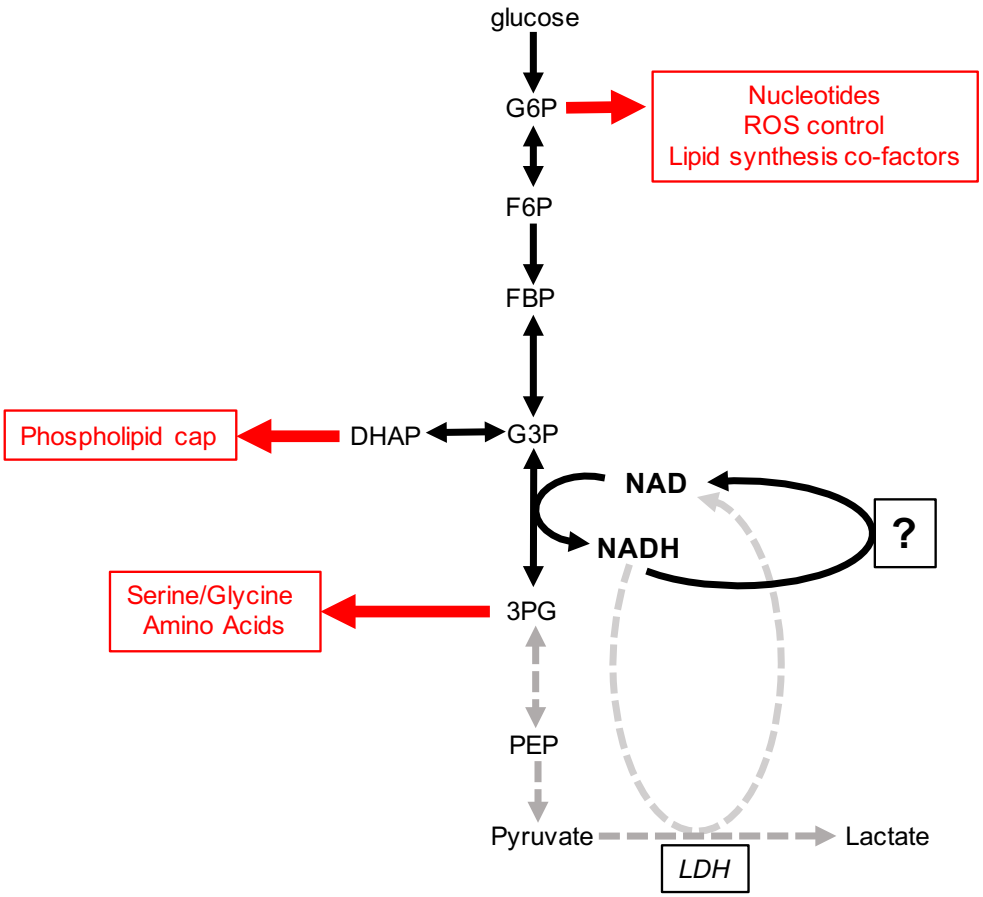

Figure 1-2. The NAD/NADH cycle in glycolysis. NAD utilized by GAPDH is thought to be regenerated by lactate dehydrogenase (LDH) in traditional Warburg models. However, glucose carbon is directed away from glycolysis to generate biomass (red). Given the reduction in glucose carbon supplied to LDH we predict there must be some alternative reaction that supports NAD regeneration in the cytosol.

early part of the twentieth century (reviewed in (Koppenol et al., 2011; Vander Heiden et al., 2009). Warburg also observed that these cells secreted an unusually high amount of acid in tandem with the increased glucose consumption (Warburg et al., 1927). The “Warburg Effect” postulates that glucose carbon is rapidly processed through glycolysis to lactate in the cytosol, precluding its participation in the TCA. Since glycolysis on its own produces two molecules of ATP per molecule of glucose, it was hypothesized that the ATP generated through accelerated glucose consumption, would suffice to meet the energetic demands lost by uncoupling the TCA and oxidative phosphorylation from glycolysis (Koppenol et al., 2011; Vander Heiden et al., 2009). The enhanced lactate production could also be explained under this hypothesis as being essential for regenerating NAD from NADH. The glycolytic enzyme glyceraldehyde 3-phosphate dehydrogenase (GAPDH) requires NAD to transfer electrons from G3P, producing NADH in the process (Figure 1-2). This NADH is compartmentally restricted and must be regenerated in the cytosol. The reduction of pyruvate to lactate by lactate dehydrogenase (LDH) serves this function, replenishing the cytosolic NAD required by GAPDH. Lactate, largely an endpoint metabolite, is secreted rapidly, and is the primary reason for the increased extracellular acidity first noted by Warburg. Thus, LDH’s ability to process pyruvate into lactate to regenerate NAD is rate limiting for glycolysis and for the cell’s ability to consume glucose. Proliferation in glycolytic ‘Warburg-like’ cells is therefore contingent upon NAD regeneration in the cytosol.

Today, the Warburg Effect is largely accepted as a universal manifestation of proliferation. Indeed, the current method for clinically identifying tumors in humans involves injecting radiolabeled glucose and imaging the body for concentrated areas of glucose consumption (Fukuda et al., 1982). Given its universal nature, aerobic glycolysis offers itself as an attractive target for therapeutic intervention in tumor cells. As a case in point, therapeutic targeting of LDHA with chemical inhibitors has recently gained momentum and is being introduced in clinical trials

(Hirschhaeuser et al., 2011; Rani and Kumar, 2016). Current technology allows us to focus in on the specific pathways involved in cancer metabolism and better understand how these pathways contribute to the physiological phenotypes noted by Warburg. As the metabolic preferences of tumors have become clearer, questions pertaining to the adequacy of LDH's capacity for NAD regeneration for aerobic glycolysis have emerged (Liberti and Locasale, 2016).

One problem with Warburg's model is stoichiometry. The Warburg hypothesis predicts that every molecule of glucose generates 2 molecules of NADH. These 2 molecules of NADH will in turn need to be turned over by LDH with 2 molecules of pyruvate to replenish the NAD. Therefore, any diversion of glucose carbon away from glycolysis would be predicted to perturb the stoichiometry and stall glucose consumption. However, as discussed previously, the utilization of glucose carbons for biomass is integral to cell division (Lunt and Vander Heiden, 2011). Based on the above, we argued that alternative mechanism(s) must exist to regenerate the NAD required to sustain increased glycolysis.

The role of glutamine in proliferative metabolism

Warburg hypothesized that glycolysis could produce enough ATP to supply the cell, and his assessment of aerobic glycolysis included the suggestion that tumor cell mitochondria were devoid of a glucose carbon supply and either defective or inactive. In fact, it is now accepted that proliferating cells harbor mitochondria that are largely functional but switch from glucose to glutamine as their primary carbon source. Glutaminolysis utilizes glutamine to generate mitochondrial alpha-ketoglutarate (αKG) in a two-step process that supplies the TCA with the carbon needed to produce NADH and drive oxidative phosphorylation (Figure 1-3a). Glutaminase (GLS), the enzyme catalyzing the initial step of glutaminolysis, is expressed in many tumor cell types in response to transcription factors that drive proliferation such as Myc (Wise et al., 2008). The up-regulation of glutaminolysis

ensures that mitochondria continue to produce ATP while glucose is utilized for production of biomass needed for generating daughter cells.

Glutamine as a source of biomass –reductive carboxylation

Glutaminolysis produces αKG which is oxidized through the TCA serving as an anaplerotic for the generation of ATP. The increased glutamine consumption during proliferation and subsequent increase in αKG levels also drives reductive metabolism through isocitrate dehydrogenase (Fendt et al., 2013b). The resulting citrate is transported out of the mitochondria into the cytosol where ATP citrate lyase acts on it to produce acetyl-coA and oxaloacetate (OAA). This acetyl-coA is a major source for lipogenesis in response to hypoxia and metformin treatment,

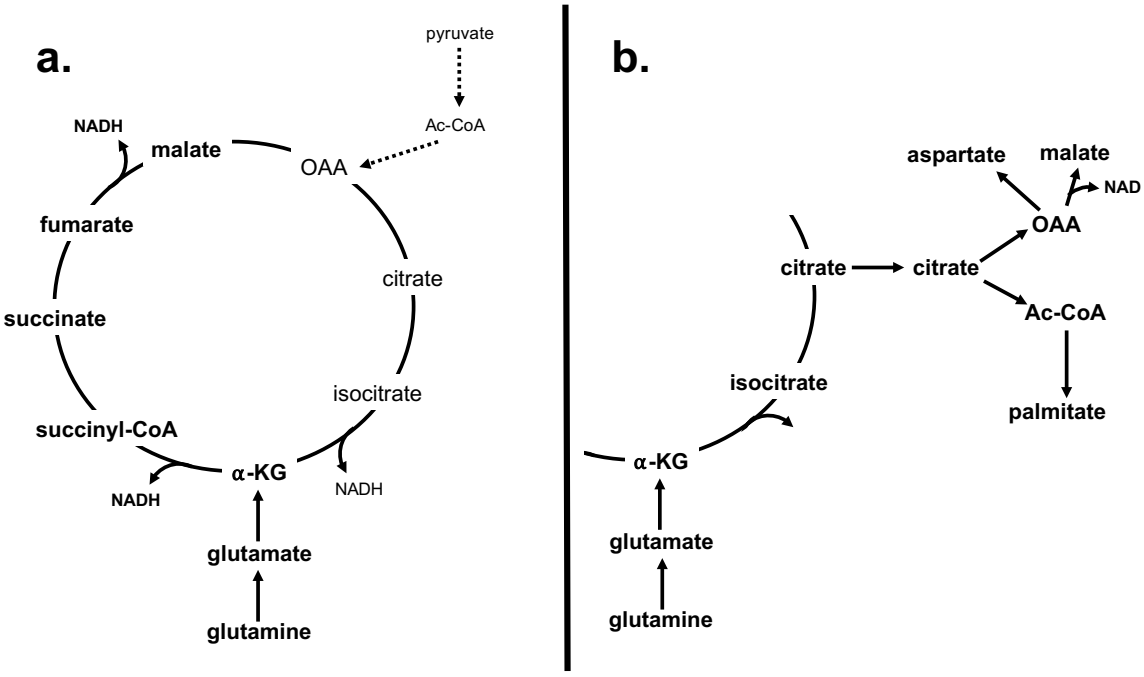

Figure 1-3. Glutamine carbon utilization during proliferation. Schematic depicting how glutamine carbon, through glutaminolysis, provides the TCA with α-ketoglutarate (a). This allows NADH production and oxidative phosphorylation to continue when glucose carbon is diverted for biomass production. The α-ketoglutarate generated from glutamine is also reductively metabolized to produce cytosolic citrate that can be utilized for biomass (b).

conditions that perturb oxidative phosphorylation (Fendt et al., 2013a; Mullen et al., 2011; Wise et al., 2011). The slowing of the TCA cycle in response to these

stresses is acutely sensed at the αKG junction, which receives carbon input from both glucose and glutamine. This results in accumulation of αKG which then drives reductive metabolism (Figure 1-3b). The breakdown of cytosolic citrate by ATP citrate lyase also generates equimolar amounts of acetyl-coA and OAA. Many studies have reported the fate of the acetyl-coA that emerges from this step (Fendt et al., 2013a; Mullen et al., 2011; Wise et al., 2011), but the fate of cytosolic OAA has been less clear.

Alpha-ketoglutarate plays a role in proliferation that is independent of metabolism

The point of intersection where both glucose and glutamine carbons contribute to the TCA cycle serves as a sensor of nutrient supply as well as demand. As such, αKG, the metabolite at this intersection, has evolved as a messenger to signal the status of the TCA to the rest of the cell. As αKG accumulates it binds to non-metabolic enzymes as a co-factor, influencing their activity. Enzymes such as the Ten eleven translocase (Tet) family of cytosine demethylases are activated by αKG eliminating epigenetic repression from gene promoters by allowing access to transcriptional machinery (Tahiliani et al., 2009). Histone demethylases, such as the Jumonji histone demethylase (JHDM), are also activated by αKG and similarly promote gene expression by relieving chromatin organization and allowing access to the transcriptional apparatus (Tsukada et al., 2006). By influencing gene expression at the level of transcription, αKG can play a direct role in cell physiology (Figure 1-4). For example, naïve stem cells maintain pluripotency by consuming glutamine to elevate levels of αKG which, in turn, maintains histone and cytosine de-methylation(Carey et al., 2015). Another recent study showed that primed human stem cells treated with exogenous αKG increase global histone and DNA demethylation and differentiate independent of mitochondrial function (TeSlaa et al., 2016). αKG is also a co-activator of prolyl hydroxylases, which utilize atmospheric oxygen to hydroxylate proline residues on target proteins. The mechanisms highlighted here provide a link between metabolic function and cell physiology that cannot be understated, especially in the context of cancer where

glutamine consumption, glutaminolysis and αKG production are significantly increased.

2-hydroxyglutarate is an oncometabolite

The significance of the influence of αKG on cell physiology in the context of cancer came to light with the identification of isocitrate dehydrogenase (IDH) mutations in human glioblastoma (Parsons et al., 2008). It was found these mutations incompletely catalyze the conversion of αKG to citrate, yielding the intermediate 2-hydroxyglutarate (Dang et al., 2009). The intracellular levels of 2-hydroxyglutarate (2-HG) increase dramatically in IDH mutant cells and outcompete αKG for co-factor

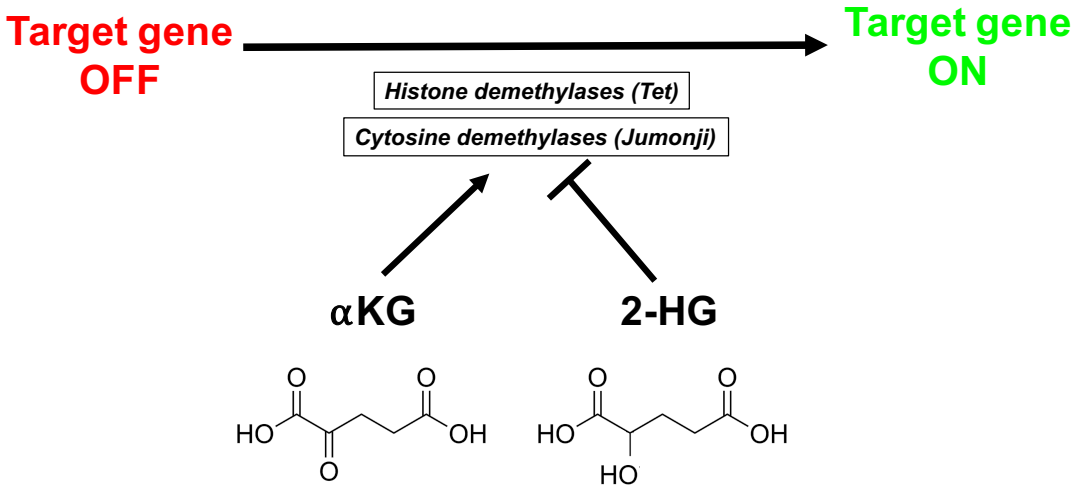

Figure 1-4. α-ketoglutarate's effect on gene expression. Increased concentrations of α-ketoglutarate in cells activate histone and cytosine demethylases. Oncogenic mutations in isocitrate dehydrogenase generate 2-hydroxyglutarate that competitively inhibit α-ketoglutarate activation of these enzymes. The repression of α-ketoglutarate activated genes appears to be critical for tumor maintenance.

activity on histone demethylases, cytosine demethylases and prolyl hydroxylases (Figueroa et al., 2010; Koivunen et al., 2012; Lu et al., 2012). The accumulated 2-HG, resulting from IDH mutations, has transformative properties and can drive tumorigenesis by competitive inhibition of αKG (Losman et al., 2013). Since the oncogenic potential of 2-HG is attributed to its competition with 'co-factor' αKG competition, it stands to reason that αKG accumulation has tumor suppressor

characteristics, although this idea has yet to be fully explored (Figure 4). Other groups have attempted to use αKG as a therapeutic in vitro and found that cell permeable αKG is toxic to some cell types (MacKenzie et al., 2007).

We set out to investigate the role other dehydrogenases may play in regenerating cytosolic NAD during Warburg metabolism. We also looked at other carbon sources for this reaction including glutamine. The dependence on glutamine, and the accompanying increase in intracellular αKG levels, led us to investigate the resistance of cancer cells to elevated levels of this tumor suppressor metabolite.

Chapter 2

MDH1 regenerates cytosolic NAD for glycolysis in proliferating cells

Introduction

Aerobic glycolysis or the Warburg Effect is defined by the increased consumption of glucose accompanied by an increased production of lactate. The consumption of NAD and production of NADH by Glyceraldehyde 3 phosphate dehydrogenase (GAPDH) is limiting to the glycolytic rate (Liberti and Locasale, 2016). The Warburg Effect necessitates uncoupling of glycolysis from the TCA cycle as lactate dehydrogenase (LDH) activity is required for the rapid regeneration of NAD to sustain a high glycolytic rate. These basic parameters have been understood and accepted for nearly a century. However, newer technologies, including mass spectrometry-based targeted metabolomics that have allowed us to trace the fate of glucose carbon during proliferation, now show that a portion of glucose carbon is diverted away from glycolysis and towards the production of biomass during proliferation. The Warburg Effect requires every molecule of glucose to be metabolized to lactate to provide GAPDH with the NAD it needs for supporting accelerated glycolysis. However, if glucose carbon is diverted to generate biomass needed for proliferation early during glycolysis, an additional source of NAD would be needed to maintain the high glycolytic rate and keep the process stoichiometrically viable. It is also important to note that lactate is a terminal metabolite which is secreted from the cell once it has served its purpose as an electron acceptor for the regeneration of NAD. We hypothesized that alternative reactions must exist to address the stoichiometry of NAD regeneration as well as allow a more efficient use of the resources available to the tumor.

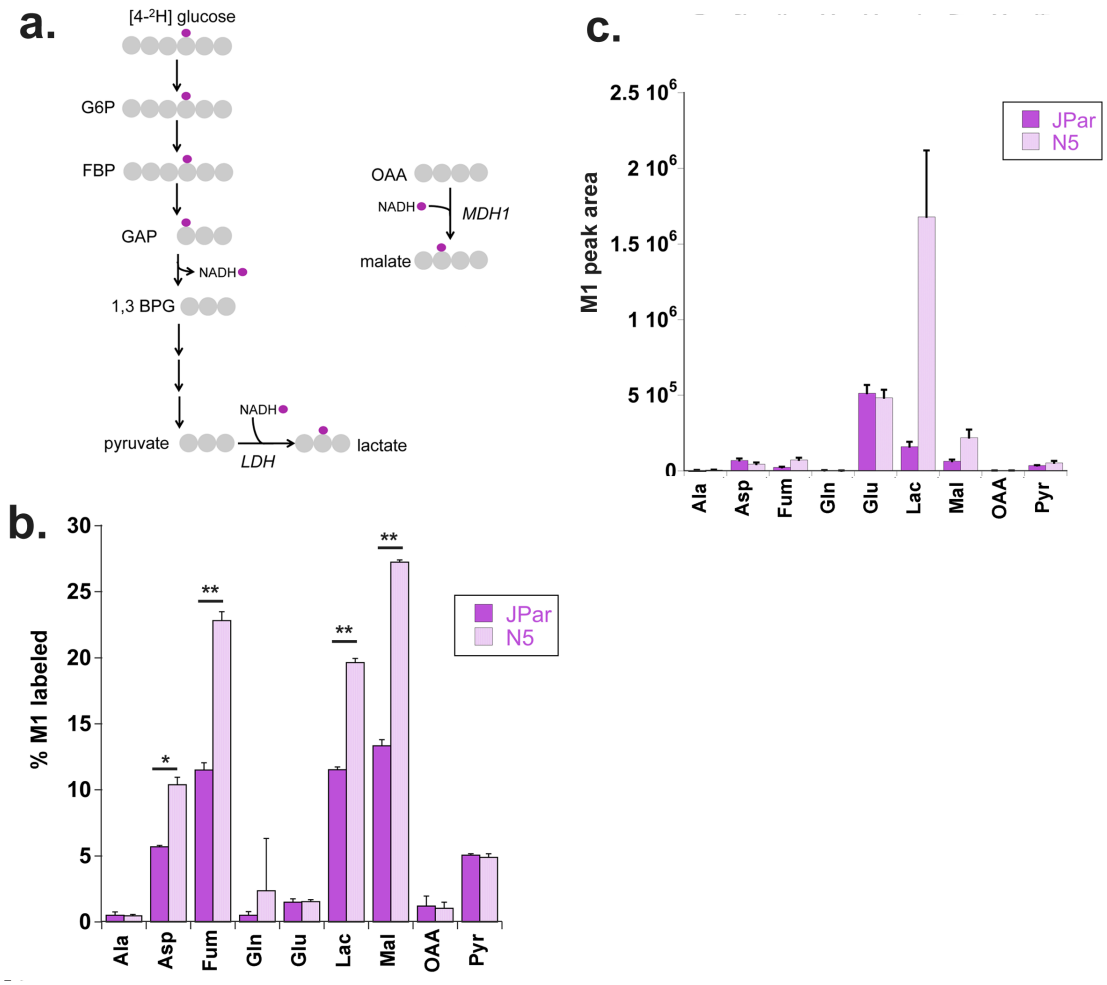

Figure 2-1. Malate dehydrogenase regenerates cytosolic NAD in cancer cells. Schematic of [^{2}H] labeling used to determine cytosolic NAD regeneration (a). Enrichment of M1 labeled metabolites from [*4-^{2}H*] *glucose* 24 hours after labeling as measured by GC-MS in JPar (baseline glucose consumption) and N5 (high glucose consumption) cells (b). Peak area of indicated M+1 metabolites indicating the relative abundance of ^{2}H incorporation in JPar and N5 cells (c). Significance was calculated using the student's T test (* $p<0.01$, ** $p<0.001$).

Results

Malate dehydrogenase 1 contributes to NAD regeneration during increased glycolysis.

Previous work from our lab had characterized a Jurkat leukemia cell model in which the over-expression of the Bcl-2 family protein Noxa increased glucose consumption and proliferative rate (Lowman et al., 2010). Despite the increased glucose consumption, the rate of glucose carbon flow to the distal steps in glycolysis decreased in the Noxa over-expressing cells, suggesting that glucose carbon was being diverted prior to the production of lactate (Lowman et al., 2010). The ideal way to assess the consequences of the Warburg effect would be to directly compare matched normal and tumor cells. However, emerging tumors acquire several genomic, transcriptomic and proteomic characteristics that confound direct comparison with normal tissue. Our Jurkat cell model of Noxa over-expression (N5), exhibits a Warburg-like phenotype following modulation of a single gene, allowing such a comparison with significantly less noise.

To investigate NAD regeneration in the Jurkat N5 Warburg model, we used ^{2}H-4 glucose which transfers the deuterium, [^{2}H], to NADH as GAPDH generates 3-phosphoglycerate from glycerol 3-phosphate (Figure 2-1a). This deuterium should then label cytosolic metabolites produced in dehydrogenase reactions that regenerate NAD downstream. We can conclude these reactions are restricted to the cytosol as no mitochondrial NADH transporters exist.

We fed cells with ^{2}H-4 glucose for 24 hours and used gas chromatography coupled mass spectrometry (GC-MS) and liquid chromatography coupled mass spectrometry (LC-MS) to trace metabolites labeled with deuterium in slowly proliferating (JPar) and highly proliferating/Warburg-like (N5) cells. We found lactate represented the largest scenario the α-carbon of aspartic acid would be predicted to be labeled with deuterium (Lamesch et al., 2007; Yang et al.,

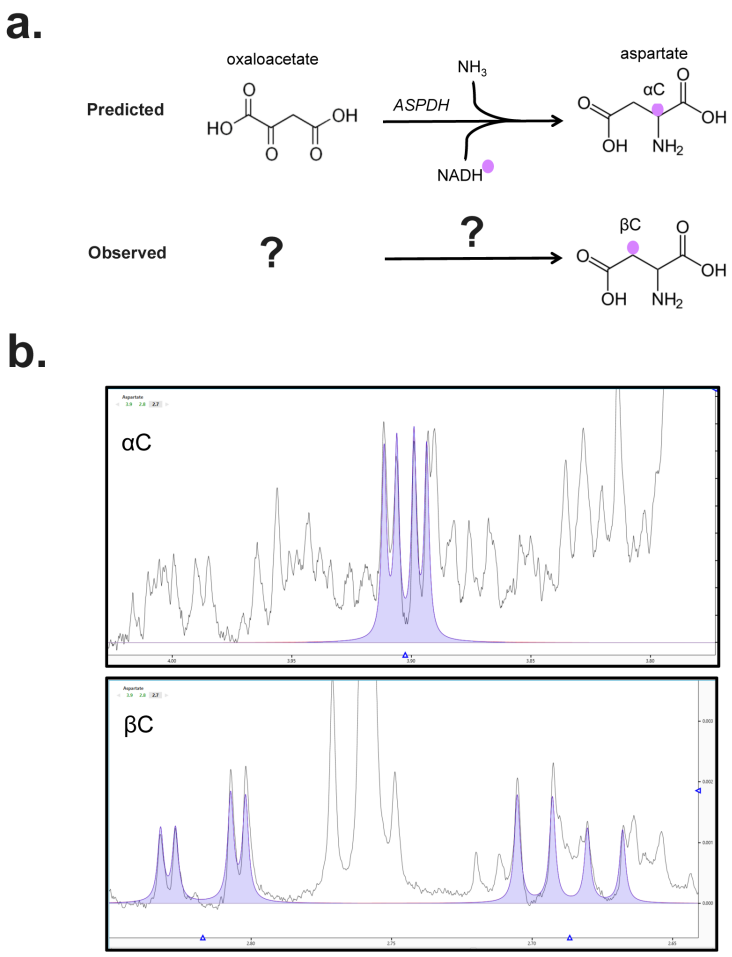

Figure 2-2. Aspartate dehydrogenase is not responsible for aspartate labeling. The aspartate dehydrogenase reaction as predicted by Yang et al in *Thermotoga maritima* and the aspartate labeling observed following [*4-*^{2}*H*] glucose labeling in N5 cells (a). NMR tracing for ^{1}H in the α and β carbon of aspartate following [4-^{2}H] glucose labeling. The partial depletion of ^{1}H on the β carbon indicates ^{2}H has replaced the ^{1}H (b).

2003)(Figure 2-2a). We performed NMR analysis to determine which carbon of aspartate was labeled (Figure 2-2b). We found that the deuterium was present not on the α-, but on the β-carbon. This could be explained by fumarate, a symmetrical molecule, returning through malate and oxaloacetate as a separate enantiomer and then to aspartate via aspartate transaminase. Thus, we concluded that both fumarate and aspartate labeling were additional metrics of malate labeling.

We used primary human T cells as an additional model to investigate MDH1 activity during proliferation. When stimulated using anti-CD3/anti-CD28 antibodies, T cells proliferate rapidly and increase aerobic glycolysis (Carr et al., 2010; Frauwirth et al., 2002). The activation of T cells also promotes the diversion of glucose carbon to support biomass synthesis (Carr et al., 2010; Frauwirth et al., 2002). We found T cells also significantly increased M1 labeling of malate after 24 hours of activation suggesting that increased MDH1 activity plays a role in robust proliferation and is not exclusive to the N5 model (Figure 2-3a).

We next looked at the flux dynamics of malate and lactate labeling in the HeLa ovarian cancer cell line which is highly glycolytic and has been used as a model for studying Warburg metabolism ((Goldberg and Colowick, 1965; Pike Winer and Wu, 2014)). Labeled malate reached steady state at 3 hours suggesting that it was the product of a robust synthesis reaction using a readily available source of oxaloacetate. Labeling dynamics for M1 malate were similar to M1 lactate, the main Warburg readout (Figure 2-3b). The malate aspartate shuttle (MAS) is a system by which NAD regeneration in the cytosol can be utilized for NADH production in the mitochondria. The MAS includes MDH1 and passes the malate into the mitochondria for MDH2 to reverse the reaction and produce mitochondrial NADH which can contribute to the electron transport chain. The role of the MAS during the Warburg effect has not yet been elucidated. We observed that HeLa cells secrete a substantial amount of labeled malate (Figure 2-3c) and this suggests in HeLa cells the malate produced by MDH1 is overwhelming other malate utilizing reactions, including the MAS. To our knowledge, this is the first evidence that malate generated in the cytosol is secreted and may contribute more to the overall extracellular acidification than previously appreciated.

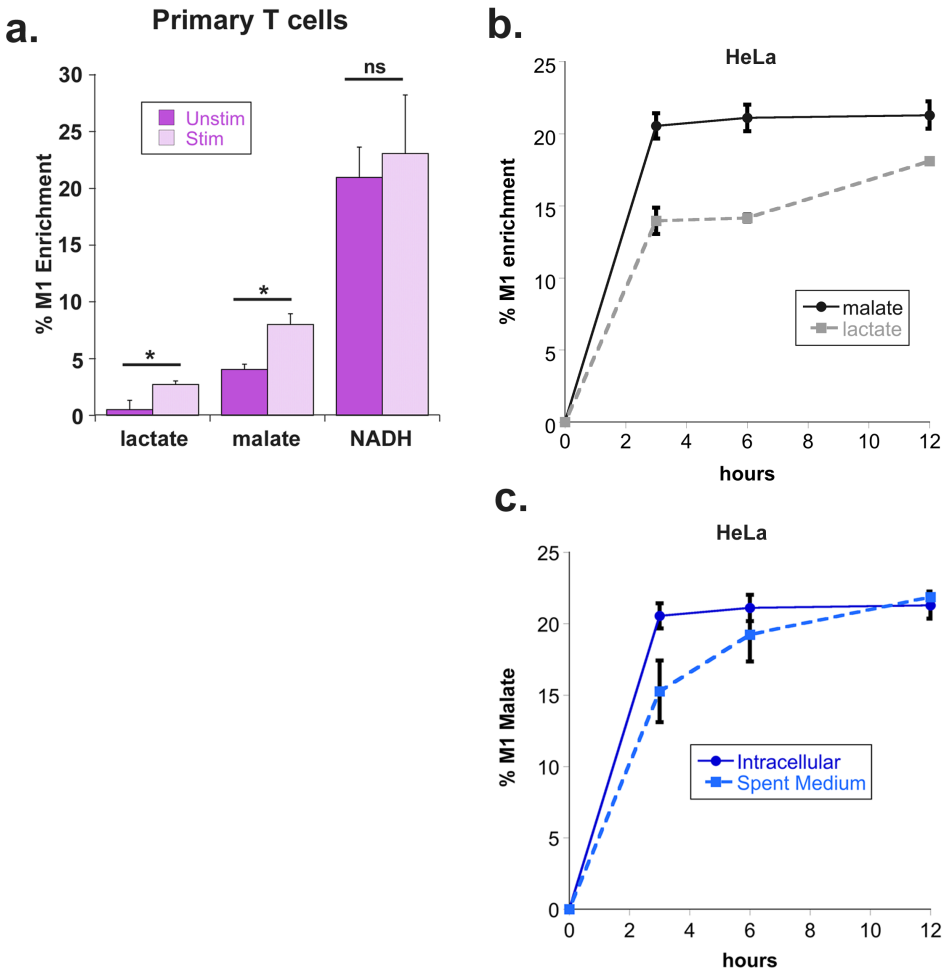

Figure 2-3. Malate dehydrogenase regenerates cytosolic NAD in primary activated T cells and HeLa cells. Primary human T cells labeled with [*4-^2H*] *glucose for* 24 hours indicate malate dehydrogenase 1 is utilized to regenerate cytosolic NAD following activation (a). Flux labeling of [*4-^2H*] *glucose in HeLa cells shows steady state is reached within 3 hours whereas lactate is still approaching steady state at 12 hours (b). Spent medium from the experiment shown in (b.) demonstrate malate is excreted from HeLa cells (c).* Significance was calculated using the student's T test (* $p<0.01$).

Deletion of Malate dehydrogenase 1 slows growth and glucose consumption

To better understand the role of MDH1 in supporting growth and glycolysis, we obtained Jurkat T-ALL cells knocked out for MDH1 by CRISPR/Cas9 (Birsoy et al., 2015). Compared to wild-type controls, MDH1 KO cells grew significantly slower and consumed less glucose per cell (Figure 2-4a-b). We reasoned that the decreased growth in MDH1 KO cells should be rescued by the addition of pyruvate. The exogenous pyruvate would supply LDHA independent of glycolytic rate and give the cell a direct substrate to restore the NAD regeneration capacity of the cell. Indeed, the addition of pyruvate rescued MDH1 deficient cells (Figure 2-4c). Overall, these data demonstrate NAD regeneration by MDH1 is critical for the proliferative capacity and glucose consumption rate of Jurkat T-ALL cells.

LDHA inhibition is only effective in the absence of MDH1.

The universal nature of the Warburg effect in proliferating cells has inspired therapeutic strategies that are aimed at limiting the glucose consumption of the tumor. One such strategy aims to cut off the NAD supply to GAPDH by targeting lactate dehydrogenase. Indeed, LDHA inhibition is a strategy that is entering clinical trials (Augoff et al., 2015; Billiard et al., 2013; Rani and Kumar, 2016). Our findings suggest the redundancy provided by MDH1 may render these therapies ineffective, at least in the context of T-ALL. To investigate this idea, we first looked at how the activity of LDHA changes when MDH1 is deleted. The basal extracellular acidification rate of MDH1 KO cells is significantly higher than that of wild-type cells, indicating that reliance on LDHA for NAD regeneration is increased in the absence of MDH1 (Figure 2-5a). We hypothesized that LDHA inhibition would have little effect on cell growth or glucose consumption in the presence of MDH1.

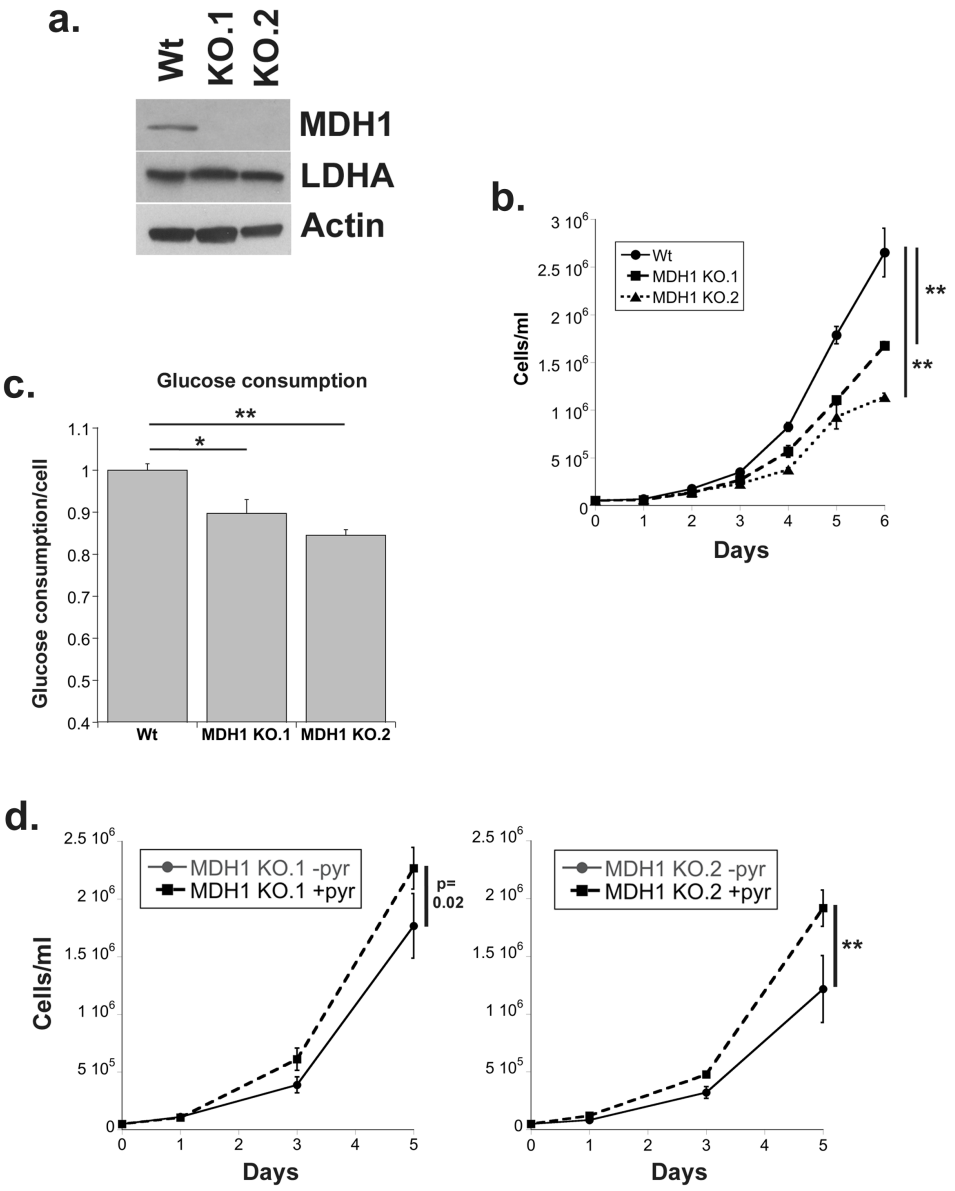

Figure 2-4. Loss of MDH1 slows proliferation and glucose consumption. Western blot showing protein expression of MDH1 and LDHA in control and MDH1 KO Jurkat cells (a). Graph shows cell number over time for indicated cell lines (b). Cells were plated at 50,000 cells per ml and counted every 24 hours. Glucose levels in the spent medium were determined on day 3 and normalized to cell number (c). MDH1 KO.1 and KO.2 cells were counted at 1, 3 and 5 days after addition of 1mM sodium pyruvate added to RPM1-1640, a pyruvate deficient medium (d). Data are the average and standard deviation of samples from experiments repeated at least three times. Significance was calculated using the student's T test (* $p<0.01$, ** $p<0.001$).

We used the LDHA inhibitor GSK2837808A which decreases lactate production (Figure 2-5b) and has been shown to inhibit the growth of colon cancer cells (Billiard et al., 2013; Xie et al., 2014). We found that in the presence of MDH1, LDHAi had no effect on cell growth. However, in the absence of MDH1, LDHA significantly decreased cell growth almost to the point of becoming cytostatic in the case of MDH1 KO.2 (Figure 2-5c).

We also observed a significant decrease in glucose consumption in MDH1 KO cells treated with LDHAi (Figure 2-5d). Interestingly, glucose consumption by wild-type cells treated with the LDHA inhibitor was dramatically increased (Figure 2-5d). As discussed earlier, the utilization of glucose carbon for lactate production is wasteful, especially during tumor emergence when access to glucose is limiting. Malate dehydrogenase 1, which provides an alternative NAD regeneration mechanism, may allow for more glucose to flow into alternative pathways. This observation also implies that oxaloacetate, the substrate for MDH1 is either readily available in the cytosol or derived from a glucose independent carbon source, or both.

These results suggest MDH1 and LDH work together in a redundant manner to regenerate NAD and support glycolysis in cancer cells, and that reliance on MDH1 could provide a proliferative advantage during the Warburg effect.

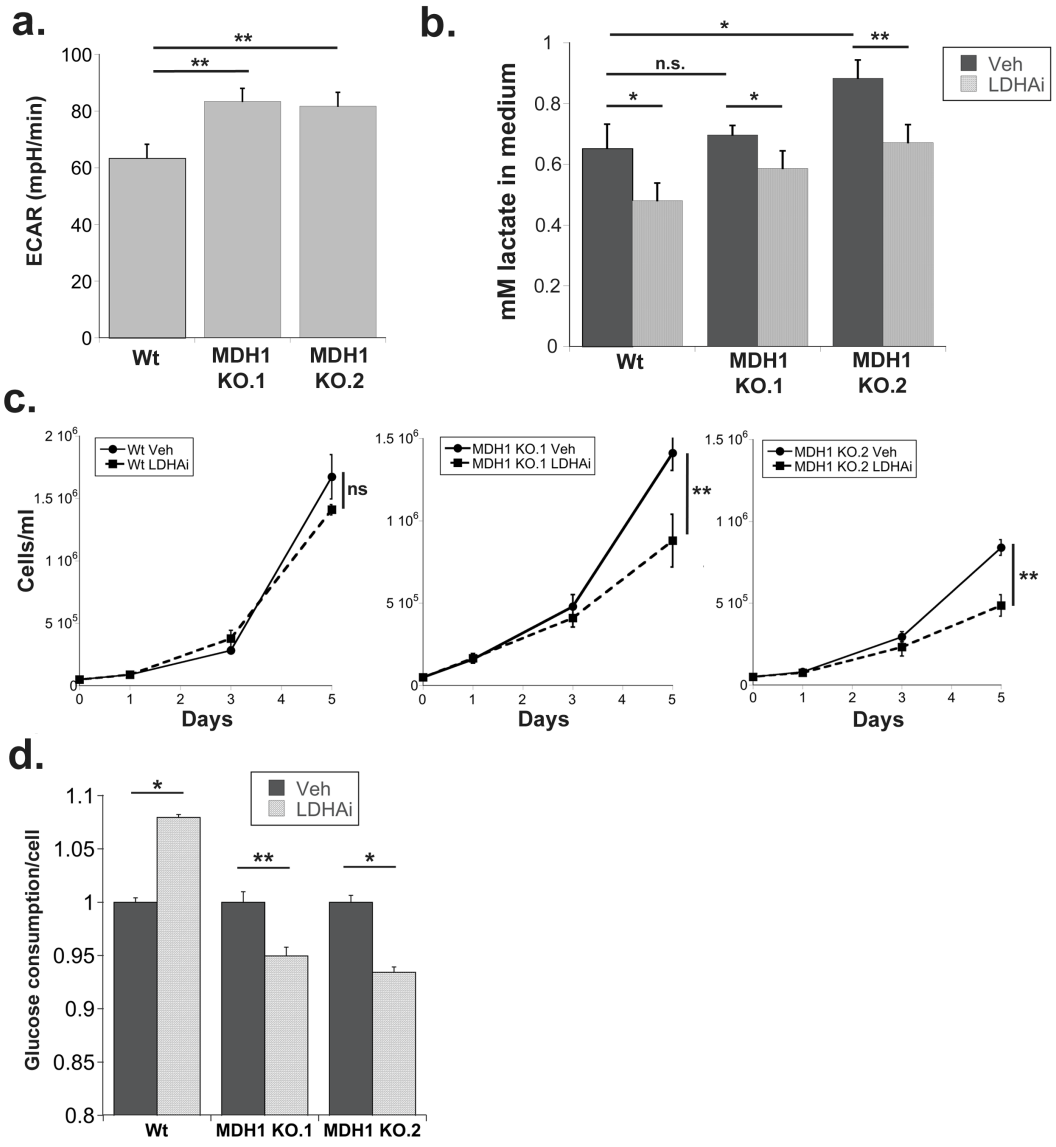

Figure 2-5. Loss of MDH1 sensitizes cells to LDH inhibition. Extracellular acidification rate measured by Seahorse in Wt and MDH1 knock-out Jurkat cells (a). Extracellular lactate levels in the medium of DMSO (Veh) or GSK2837808A (LDHAi) treated cells 48 hours after administration and normalized to cell number (b). Cell concentrations on the indicated days following treatment with either DMSO (Veh) or GSK2837808A (LDHAi) (c). Glucose levels in the spent medium from day 3, normalized to cell number and shown relative to levels detected in vehicle treated cell medium (d). Data are the average and standard deviation of samples from experiments repeated at least twice. Significance was calculated using the student's T test (* $p<0.01$, ** $p<0.001$).

MDH1 amplification is prominent in human tumors and correlates with poor prognosis.

Our data suggested MDH1 provided a benefit to tumor growth and glucose consumption. Thus, we hypothesized human tumors would benefit from *MDH1* amplification. We queried The Cancer Genome Atlas using the cBioportal (Cerami et al., 2012; Gao et al., 2013) to investigate incidences of genomic aberrations in the *MDH1* gene. We found that *MDH1* was rarely mutated suggesting functional MDH1 enzymatic activity is prominent in human tumors (Figure 2-6a). We found that amplification was the most common genomic aberration, with occurrence as high as 11% in lung squamous cell carcinoma. (Figure 2-6b). Patients within this dataset with genomic amplification of *MDH1* showed more than a 50% decrease in survival rate suggesting MDH1 amplification correlates with more aggressive tumors (Figure 2-6c). The *MDH1* gene is located on chromosome 2p13 which has not been reported to be a common amplification segment and is not adjacent to known oncogenes. Rather, we argue *MDH1* amplification is an acquired aberration that provides a proliferative benefit by enhancing the ability to process glucose for biomass production. When we queried *MDH1* aberrations in tandem with *LDHA*, we found that *MDH1* was amplified more frequently than *LDHA* in all the tumor types we investigated (Figure 2-6d). Furthermore, these amplification events were mutually exclusive underscoring the redundancy of these enzymes (Figure 2-6d). The frequency of *MDH1* amplification events and aggressive nature of *MDH1* over-expressing tumors help validate the hypothesis that *MDH1* plays an important role in supporting tumor proliferation.

We next asked whether the over-expression of MDH1 was sufficient to accelerate anchorage independent growth, a readout for tumorigenicity. We used the A549 lung cancer model which has been reported to be highly dependent on LDHA inhibition (Liu et al., 2014; Xie et al., 2014). We found that stable over-expression of MDH1 in A549 cells (Figure 2-7a) significantly increased the number of colonies formed in soft agar indicating that MDH1 expression

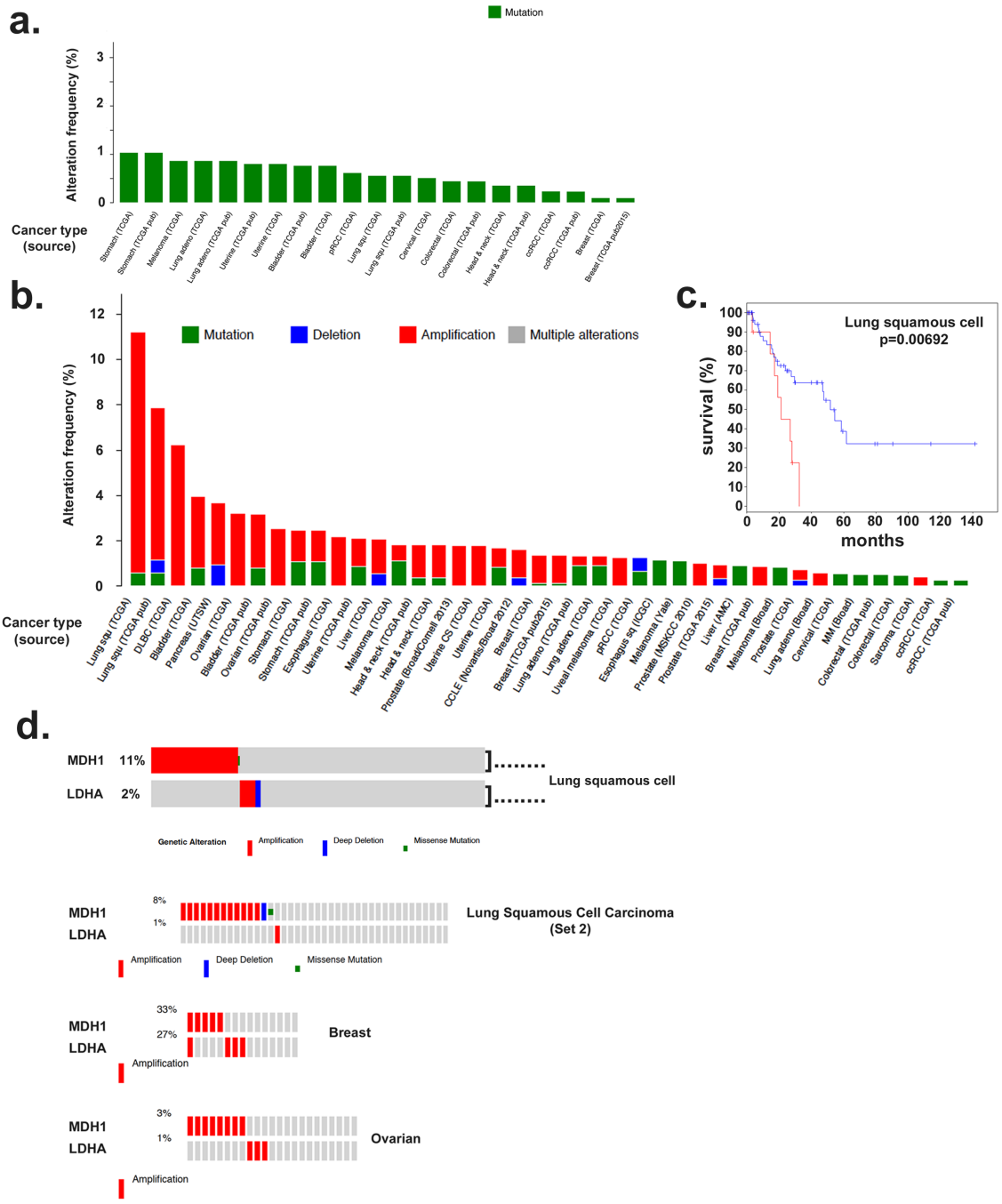
a.
Mutation
Alteration frequency (%)
Cancer type (source)
b.
Mutation
Deletion
Amplification
Multiple alterations
Alteration frequency (%)
Cancer type (source)
c.
Lung squamous cell
p=0.00692
survival (%)
months
d.
MDH1 11%
LDHA 2%
Lung squamous cell
Genetic Alteration
Amplification
Deep Deletion
Missense Mutation
MDH1
LDHA
8%
1%
Lung Squamous Cell Carcinoma (Set 2)
Amplification
Deep Deletion
Missense Mutation
MDH1
LDHA
33%
27%
Breast
Amplification
MDH1
LDHA
3%
1%
Ovarian
Amplification

Figure 2-6. MDH1 is amplified in human cancers and correlates with poor prognosis. The Cancer Genome Atlas online database was queried using cBioportal software to query *MDH1* mutations (a). All MDH1 expression aberrations, including amplification, deletions and mutations in human tumors were queried (b). The lung squamous cell carcinoma subset was further interrogated to correlate *MDH1* amplification with disease free survival (c). *MDH1* and *LDHA* queried together for genomic aberrations in the lung squamous cell carcinoma dataset (d).

increases anchorage independent cell growth (Figure 2-7b). These data also predict that relieving dependence on LDHA with MDH1 is a potential mechanism of resistance to therapeutic targeting of LDHA. Next, we wanted to determine whether the proliferative rate of MDH1 KO cells could be rescued by restoring MDH1 expression. Stably re-expressed MDH1 in MDH1 KO.2 cells significantly restored the proliferative rate (Figure 2-7c).

Taken together, these results demonstrate that over-expression or amplification of MDH1 provides a proliferative advantage to cancer cells.

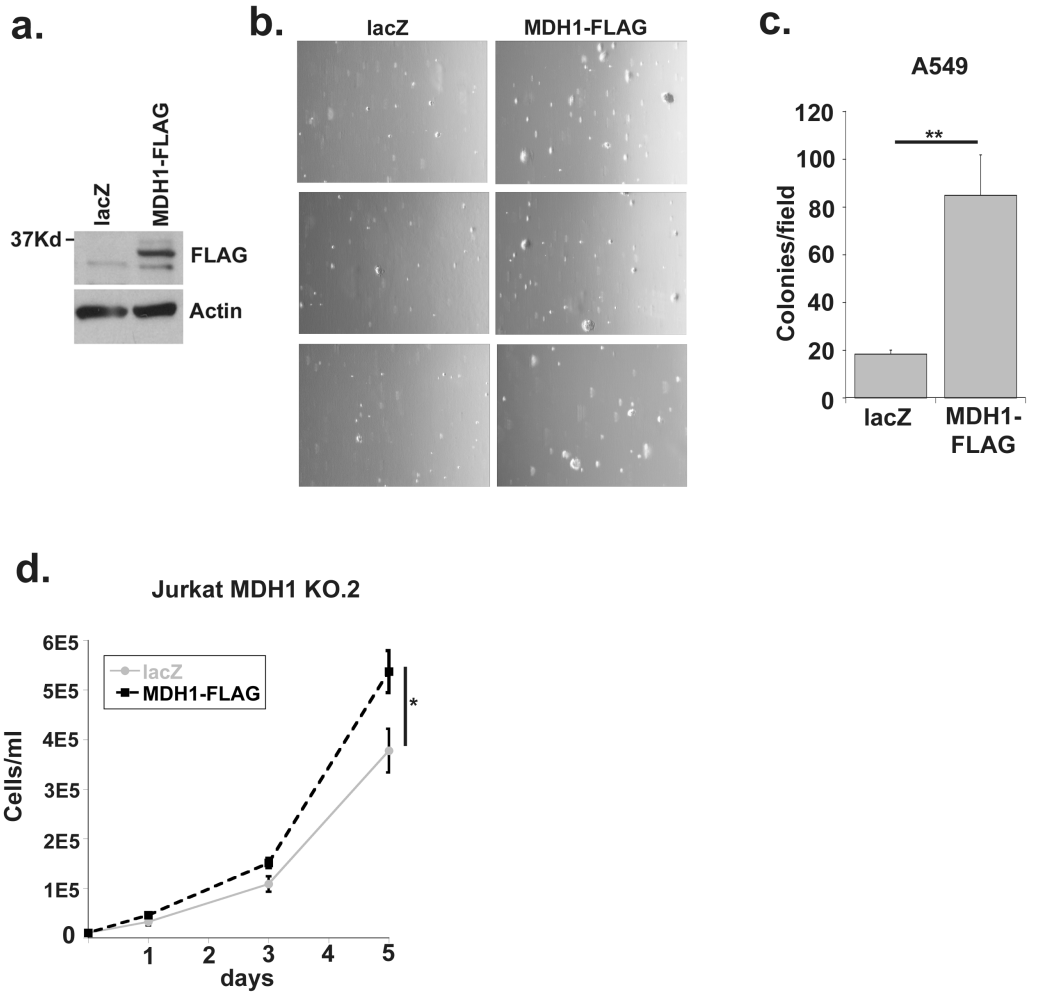

Figure 2-7. MDH1 over-expression increases anchorage independent growth. Western blot demonstrating expression of MDH1-FLAG in stably transfected A549 cell lines (a). Representative low magnification microscopic images of colony numbers and sizes at 14 days (b). Colony counts after 2-week soft agar colony formation assays. The average number of colonies from ten low-magnification microscopic fields from triplicate wells is shown (c). MDH1 KO.2 Jurkat cells were stably transfected with MDH1-FLAG or lacZ and plated at 10,000 cells per ml. Cell concentration was plotted on days 1, 3 and 5 (d). Data represented are the average and standard deviation of triplicate samples from a representative experiment repeated at least twice. Significance was calculated using the student's T test (* $p<0.01$, ** $p<0.001$).

Conclusions

In this chapter, we demonstrate that malate dehydrogenase 1 activity supports the regeneration of NAD during aerobic glycolysis in proliferating cells and in cancer. Limiting the glucose uptake potential of a cancer cell is an attractive therapeutic strategy as the Warburg phenomenon is a nearly universal hallmark of tumors. Currently the field is looking to target the cytosolic NAD regenerating capacity of the tumor cell with the goal of limiting the cell's ability to process glucose and slow down its consumption. Current glycolysis targeting strategies are focused on the NAD regenerating enzyme lactate dehydrogenase. Our findings suggest that malate dehydrogenase 1 intervention will also be required to fully limit the NAD regeneration potential of the cell. Besides, the inhibition of LDHA will likely drive resistance through MDH1. Our results, as well as data from TCGA suggest the switch to MDH1 could result in more aggressive tumors that use a more efficient pathway of glucose independent carbon to regenerate NAD. The product of the MDH1 reaction, malate, is a substrate for many other catabolic reactions beneficial for proliferation.

The next step was to determine the carbon source for the MDH1 reaction. Oxaloacetate, the substrate for MDH1 is likely independent of glucose as forcing cells to utilize MDH1 results in more robust glucose consumption (Figure 2-6d). The source of oxaloacetate is also readily available in the cytosol as demonstrated by labeling dynamics which had indicated that M1 malate labeling from ^{2}H 4-glucose reached steady state by three hours. We set out to identify the source of cytosolic OAA used by MDH1 to produce malate and regenerate NAD.

Chapter 3

Cytosolic MDH1 utilizes glutamine-derived carbons to support glycolysis

Introduction

The findings described in the previous chapter demonstrate a critical role for malate dehydrogenase 1 (MDH1) in the regeneration of cytosolic NAD to sustain the increased glycolysis associated with proliferation. We were interested in the carbon source of cytosolic oxaloacetate (OAA), the MDH1 substrate. Flux experiments had suggested the substrate for the MDH1 reaction was not only readily available but likely to be independent of glucose carbon. Thus, we surmised that MDH1 must use alternative carbon sources to produce malate and cytosolic NAD. Besides glucose, glutamine is a major carbon source for the citric acid cycle in proliferating cells. Glutamine, like glucose, is abundant in the blood. Although it is a non-essential amino acid, proliferating cells prefer increasing the uptake and breakdown of exogenous glutamine to generating it *de novo*. Glutamine carbon is metabolized via glutaminolysis in two steps to alpha-ketoglutarate (αKG) which enters the TCA cycle in the mitochondria. The diversion of glucose carbon to lactate production during the Warburg effect renders essential the use of glutamine-derived αKG as an anaplerotic for maintaining the TCA cycle and for oxidative phosphorylation. Interestingly, the rate of oxidative phosphorylation decreases substantially in proliferating cells suggesting glutamine is also metabolized via alternative routes (Fendt et al., 2013b; Lum et al., 2007; Wise et al., 2011). Glutamine carbons, much like those of glucose, support both energy production as well as the biosynthesis of nucleotides, amino acids and NADPH that are so critical for proliferation. Next, we investigated the role of glutamine in providing carbon for the MDH1 reaction.

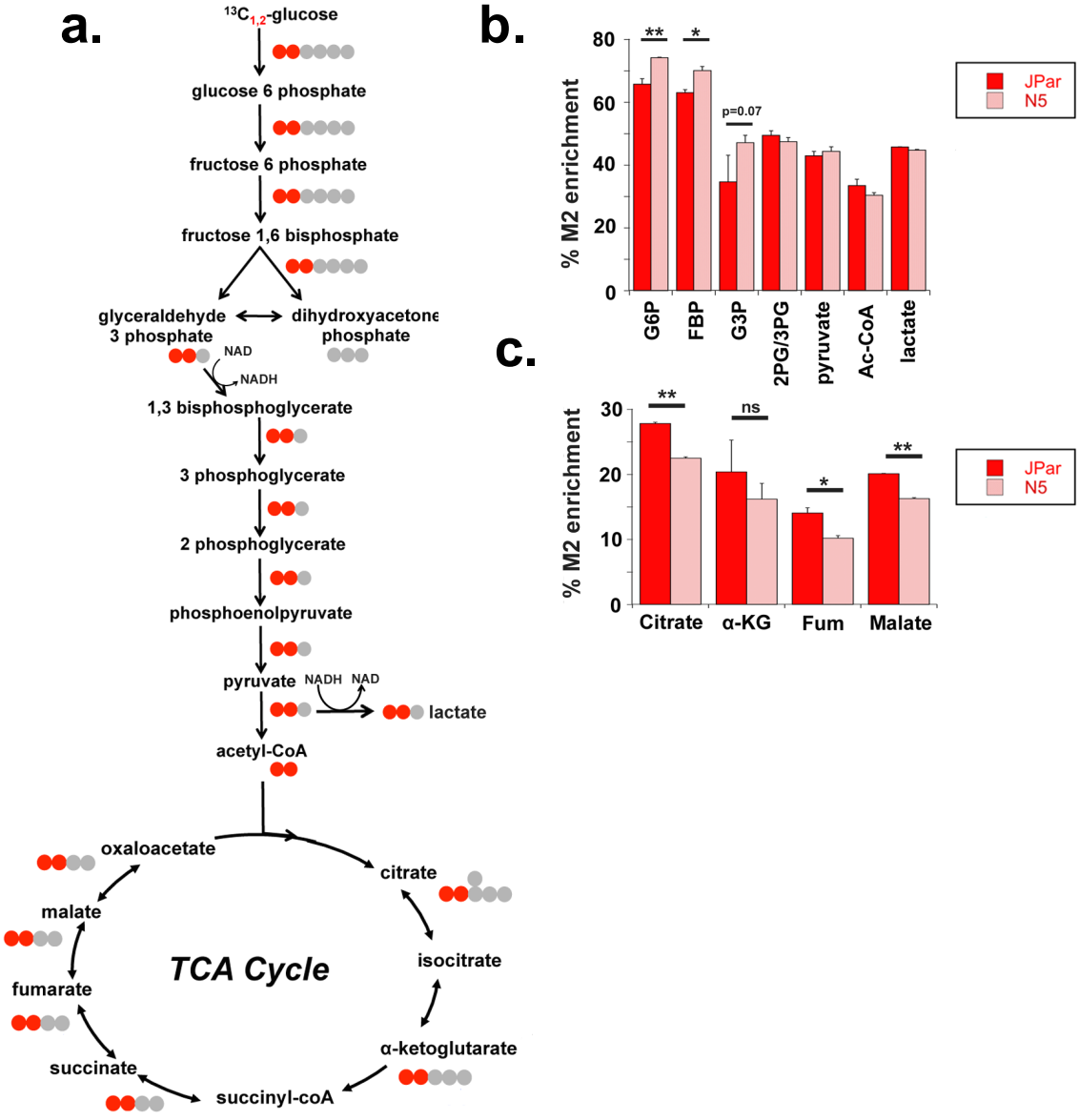
a.
$^{13}C_{1,2}$-glucose
glucose 6 phosphate
fructose 6 phosphate
fructose 1,6 bisphosphate
glyceraldehyde 3 phosphate
dihydroxyacetone phosphate
NAD
NADH
1,3 bisphosphoglycerate
3 phosphoglycerate
2 phosphoglycerate
phosphoenolpyruvate
pyruvate
NADH
NAD
lactate
acetyl-CoA
oxaloacetate
citrate
isocitrate
α-ketoglutarate
succinyl-coA
succinate
fumarate
malate
TCA Cycle
b.
% M2 enrichment
80
60
40
20
0
**
*
p=0.07
G6P
FBP
G3P
2PG/3PG
pyruvate
Ac-CoA
lactate
JPar
N5
c.
% M2 enrichment
30
20
10
0
**
ns
*
**
Citrate
α-KG
Fum
Malate
JPar
N5

Figure 3-1. Noxa over-expressing cells increase glycolysis but not lactate production from glucose. Schematic tracing the incorporation of [^{13}C] label from [1,2-^{13}C] glucose (red) through glycolysis and the TCA cycle, and [U-^{13}C] glutamine (blue) into TCA cycle metabolites (a). Glycolysis metabolites labeled from [1,2-^{13}C] glucose following 24 hours of labeling, shown as a percentage of total metabolite measured using LC/MS (b). G6P: glucose 6 phosphate, FBP: fructose 1,6 bisphosphatase, G3P: glyceraldehyde 3 phosphate, 2PG/3PG: phosphoglycerate. TCA metabolites labeled from glucose carbon measured via LC/MS following 24 hours of labeling (c). Data represented are the average and standard deviation of triplicate samples from a representative experiment repeated at least twice. Significance was calculated using the student's T test (* $p<0.01$, ** $p<0.001$).

Results

Glucose carbon is diverted prior to lactate in Noxa over-expressing cells.

In a previous study, we showed Noxa over-expressing cells (N5) consumed glucose faster than controls but much of that glucose failed to complete glycolysis (Lowman et al., 2010). This suggested the increased glucose carbon consumed by N5 cells was diverted into alternative pathways. To gain better insight into how glucose was utilized in N5 cells we used ^{13}C-1,2 glucose to trace the fate of glucose carbons (Figure 3-1a). We found N5 cells increased the percentage of labeled pool (M+2) in early glycolysis as far as the glyceraldehyde 3 phosphate dehydrogenase (GAPDH) reaction, but not beyond, and decreased overall glucose carbon contribution to the TCA (Figure 3-1b-1c). These data are consistent with a previous study from our lab showing a reduction in the amount of ^{3}H water produced in the phosphenolpyruvate step in ^{3}H-glucose labeled N5 cells compared to JPar controls (Lowman et al., 2010), suggesting that lactate dehydrogenase was not being supplied with sufficient glucose carbon to sustain increased glycolysis beyond the GAPDH step. N5 cells diverted a significant amount of glucose carbon into the pentose phosphate pathway (PPP) that supplies NADPH for the control of reactive oxygen species (ROS) and *de novo* lipogenesis. Two molecules of NADPH are generated from every molecule of glucose 6 phosphate that enters the PPP.

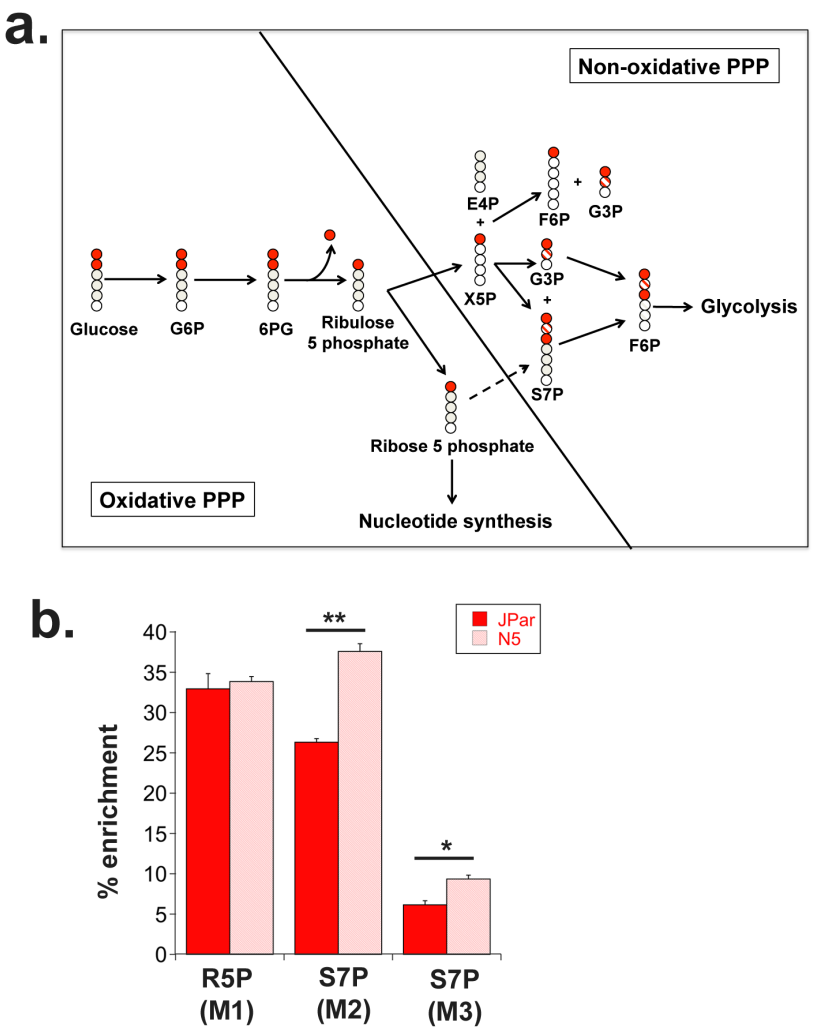

Figure 3-2. Noxa over-expressing cells direct glucose carbon into the pentose phosphate pathway. Simplified schematic diagram of the pentose phosphate pathway (PPP) tracing glucose carbons through portions of the oxidative and non-oxidative arm (a). Noxa overexpressing cells increase glucose carbon flux to the non-oxidative phase of the pentose phosphate pathway (b). Experiments were performed as in Figure 4 using [1,2-^{13}C] D-glucose as a label. Shown is percent enrichment of M1 label from glucose into R5P and M2/M3 into S7P per the schematic in (a). R5P: ribose 5 phosphate/ribulose 5 phosphate (oxidative PPP metabolite). S7P: sedoheptulose 7 phosphate (non-oxidative PPP metabolite).

However, the carbon from the PPP is limited to two fates. The oxidative path results in the generation of ribose 5 phosphate (R5P), used for the generation of *de novo* nucleotides. The other (non-oxidative) option returns the carbon to glycolysis (Figure 3-2a). We found N5 cells increased glucose carbon to sedoheptulose 7 phosphate (S7P, non-oxidative), but not to R5P (oxidative), indicating that the non-oxidative arm of the PPP is accelerated in these cells (Figure 3-2b). Furthermore, these results suggest that some of the carbon lost to the PPP returns to glycolysis.

Noxa overexpressing cells utilize glutamine carbon for TCA and for cytosolic metabolites generated through reductive carboxylation.

Since N5 cells did not metabolize glucose carbon beyond G3P or into the TCA cycle, (Figure 3-1c) we asked whether glutamine served as an alternative carbon source for the TCA in these cells. Many cancer cells and proliferating normal cells are dependent on glutamine as a carbon source for both biomass production as well as TCA metabolism (Fendt et al., 2013b; Lum et al., 2007; Wise et al., 2011) (Figure 3-3a). We fed N5 and JPar cells with ^{13}C-U glutamine and traced the fate of ^{13}C using targeted metabolomics. We found that rate of glutamine uptake was similar in both cell types (Figure 3-3b). However, N5 cells increased the rate of conversion of glutamine to glutamate as well as to TCA intermediates αKG, fumarate and malate. Thus, N5 cells utilize glutamine carbon to support the continued activity of the TCA cycle when glucose carbon is diverted to anabolic processes for generating biomass.

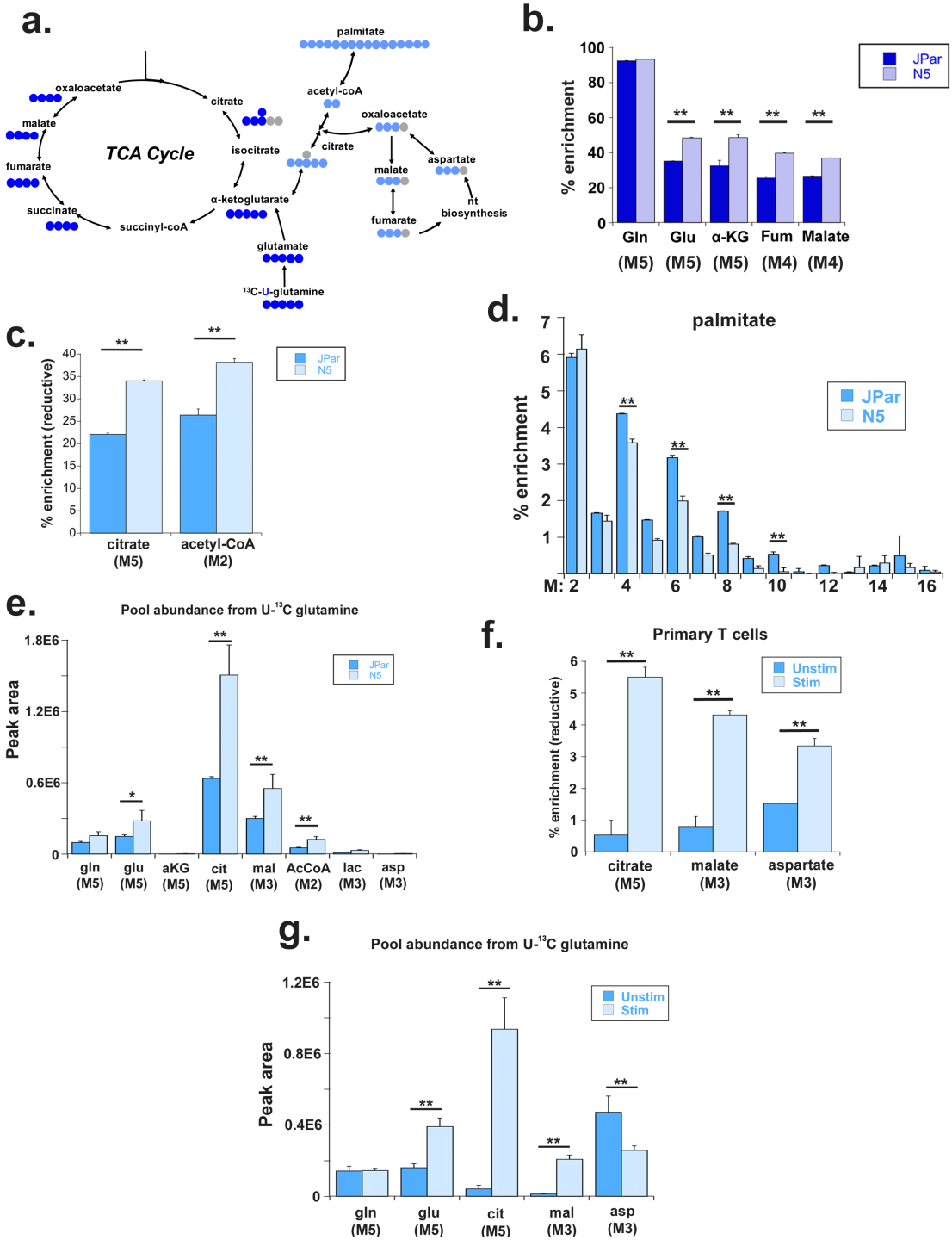
a.
palmitate
acetyl-coA
oxaloacetate
citrate
malate
TCA Cycle
isocitrate
citrate
oxaloacetate
fumarate
malate
aspartate
α-ketoglutarate
succinate
succinyl-coA
fumarate
nt biosynthesis
glutamate
13C-U-glutamine
b.
% enrichment
JPar
N5
Gln (M5)
Glu (M5)
α-KG (M5)
Fum (M4)
Malate (M4)
c.
% enrichment (reductive)
citrate (M5)
acetyl-CoA (M2)
d.
palmitate
% enrichment
M: 2 4 6 8 10 12 14 16
e.
Pool abundance from U-13C glutamine
Peak area
gln (M5)
glu (M5)
aKG (M5)
cit (M5)
mal (M3)
AcCoA (M2)
lac (M3)
asp (M3)
f.
Primary T cells
Unstim
Stim
% enrichment (reductive)
citrate (M5)
malate (M3)
aspartate (M3)
g.
Pool abundance from U-13C glutamine
Peak area
gln (M5)
glu (M5)
cit (M5)
mal (M3)
asp (M3)

Figure 3-3. Noxa over-expressing cells increase reductive carboxylation of glutamine to support cytosolic malate production. Schematic tracing the incorporation of [^{13}C] label from [U-^{13}C] glutamine metabolized in oxidative (royal blue) and reductive (light blue) directions (a). Enrichment of glutaminolytic and TCA metabolites derived from [U-^{13}C] glutamine following 24 hours of labeling, detected using LC/MS (b). Gln: glutamine, Glu: glutamate, αKG: alpha-ketoglutarate, Fum: fumarate. Number of labeled carbons is indicated in parentheses. Percent enrichment of citrate and acetyl-CoA derived from reductive carboxylation of [U-^{13}C] glutamine 24 hours after labeling, determined via LC/MS (c). Percent enrichment of glutamine carbon into palmitate (d). Pool abundance of indicated metabolites in JPar and N5 cells quantified by peak area and normalized to sample protein concentration (e). Percent enrichment of citrate, malate and aspartate derived from reductive carboxylation of [U-^{13}C] glutamine in primary human T cells 24 hours after labeling and activation. (f) Pool abundance of indicated metabolites in unstimulated and stimulated primary human T cells quantified by peak area and normalized to sample protein concentration. Isotopomer label indicated in parenthesis below metabolites. Data presented are the average and standard deviation of triplicate samples from a representative experiment repeated at least twice. Significance was calculated using the student's T test (* $p<0.01$, ** $p<0.001$).

Glutamine metabolism in proliferating cells has also been shown to be important for biomass production. One particularly important step for glutamine metabolism is the reductive carboxylation of mitochondrial αKG into citrate (Figure 3-3a). IDH enzymes catalyze this reaction bi-directionally and are therefore, dependent on the αKG citrate ratio in the mitochondria (Fendt et al., 2013b). As proliferating cells increase glutamine consumption and αKG production through glutaminolysis, the direction of αKG metabolism can vary. The excess citrate generated by reductive carboxylation is exported into the cytosol where it is broken down into acetyl-CoA and oxaloacetate. The acetyl-CoA generated in this manner has been shown to be a major substrate for lipid synthesis in tumor cells (Wise et al., 2011). However, the fate of the OAA is less clear although cytosolic OAA would be predicted to be a substrate for MDH1.

We calculated the total pools of αKG and citrate in JPar and N5 cells. Finding the αKG to citrate ratio was 33% higher in N5 cells (not shown) we reasoned that the reductive carboxylation of glutamine could play a role in providing the OAA substrate for MDH1 in the cytosol. Labeling with ^{13}C-U glutamine allows for evaluating of both oxidative and reductive αKG metabolism (Figure 3-3a). We

found N5 cells increased the production of reductively generated citrate and acetyl-CoA (Figure 3-3c). Although our assay was unable to identify OAA, acetyl-CoA and OAA are 1:1 with the lysis of citrate. This acetyl-CoA is often the substrate for *de novo* lipogenesis in other cancer cells. However, we found instead that N5 cells decreased incorporation of reductively generated acetyl-CoA into palmitate (Figure 3-3d). The fate of the acetyl-CoA produced from the reductive carboxylation of glutamine remains unclear. We argue that the breakdown of citrate in N5 cells was aimed at OAA production rather than acetyl-CoA.

We next looked at downstream metabolism of the OAA that was produced by reductive carboxylation of glutamine. N5 cells significantly increased percent enrichment of glutamine carbon into malate, but not into aspartate, demonstrating glutamine carbon is a source for the MDH1 reaction and increases during aerobic glycolysis. Importantly, the peak areas for the reductive metabolism of glutamine carbon demonstrate a clear increase in labeled pool totals for the pathway leading to MDH1 (Figure 3-3e). Primary activated T cells also increase MDH1 activity in parallel with aerobic glycolysis (Figure 3-3f). We found that stimulation of T cells also produced a significant amount of cytosolic malate through reductive carboxylation. Interestingly, although the percentage of labeling of reductively generated aspartate significantly increased in stimulated T cells, the pool size of labeled aspartate was lower suggesting the fate of cytosolic OAA favored MDH1 over aspartate transaminase (Figure 3-3g). Overall, these data demonstrate that the increased activity of MDH1 during aerobic glycolysis, is fueled by OAA generated through the reductive carboxylation of glutamine.

Jurkat cells require MDH1 for dependence on glutamine.

Our previous findings suggest flux through reductive carboxylation was a major draw for glutamine carbon and that OAA from glutamine was supplying MDH1 with the ability to regenerate cytosolic NAD and support glycolysis. To further test this idea, we cultured MDH1 wt and KO cells in medium with low or high

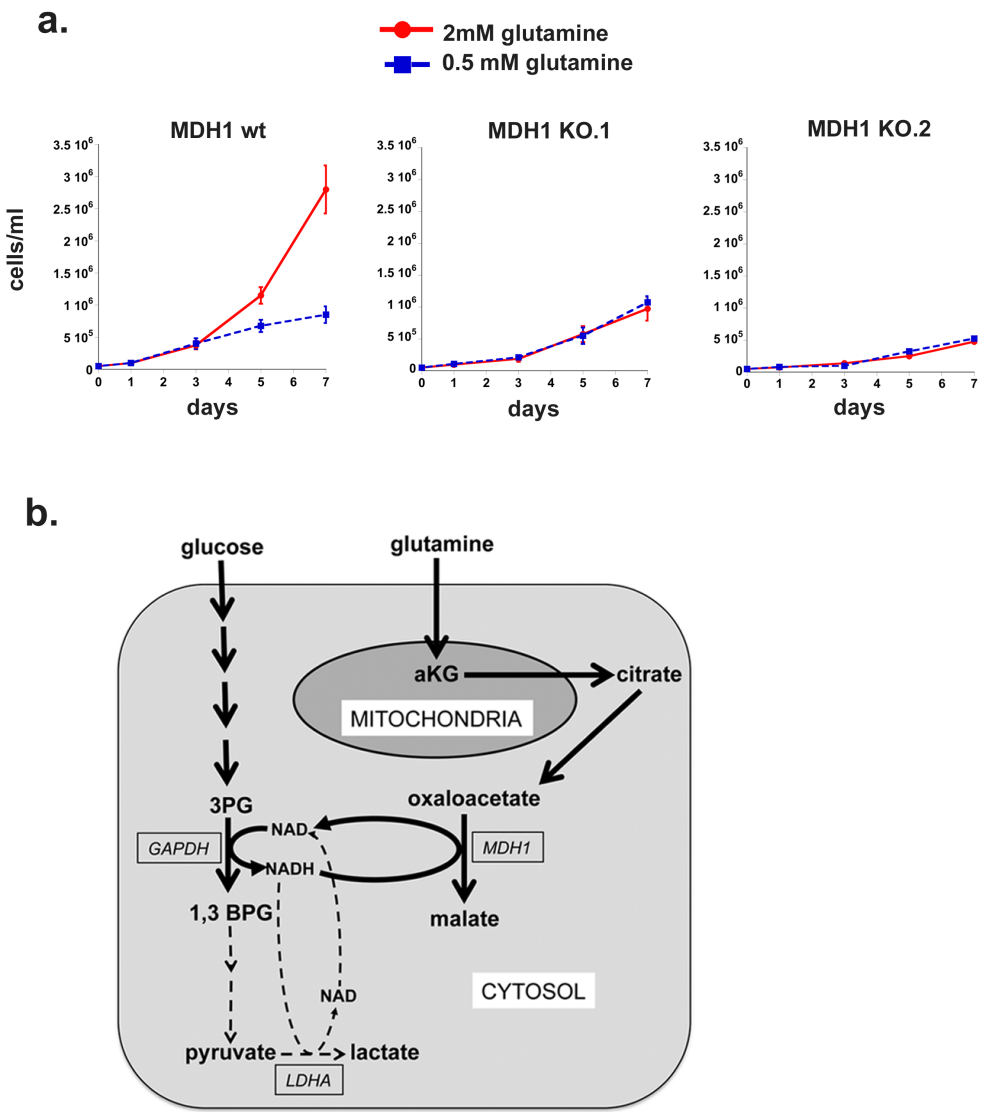

Figure 3-4. Glutamine dependence is lost in MDH1 knock out cells. MDH1 wild-type and knock-out cells were cultured in normal (2mM) or low (0.5mM) glutamine for 7 days. Cells were counted at 1, 3, 5 and 7 days. Data presented are the average and standard deviation of quadruplicate samples from a representative experiment repeated at least twice (a). Simplified model to show how malate dehydrogenase 1 and glutamine help support the increased glucose uptake and glycolysis by replenishing the NAD consumed by the GAPDH catalyzed step, a function primarily attributed to LDH activity in highly glycolytic cells. Our studies suggest that, in proliferating cells, MDH1 is a significant alternative source of cytosolic NAD, utilizing the carbons from the reductive carboxylation of glutamine for the NADH dependent synthesis of malate (b).

glutamine and monitored their growth. Only MDH1 wt cells were sensitive to low glutamine concentrations supporting the idea that a major source of glutamine carbon in proliferating cells is the MDH1 reaction (Figure 3-4a).

Conclusions

Glutamine is well recognized as a critical carbon source during proliferation (Fendt et al., 2013b; Lum et al., 2007; Wise et al., 2011). The oxidation and reductive metabolism of glutamine carbon have both been reported to play significant roles in proliferative metabolism. Here, we demonstrate a new role for glutamine carbon in supporting glycolysis. By supplying cytosolic oxaloacetate for NAD regeneration by MDH1, glutamine carbon helps support the increased glucose consumption and biomass production in proliferating cells. Previous studies have reported that the primary role of reductive carboxylation of glutamine was to provide the acetyl-CoA needed for *de novo* lipogenesis (Lum et al., 2007; Wise et al., 2011), but little was known about the contribution of oxaloacetate, the other by-product of citrate lysis. Our studies are the first to suggest that the role of reductive carboxylation extends beyond supplying acetyl-CoA for lipid generation to include provision of carbon substrates for MDH1 activity. Using glutamine carbons for cytosolic NAD regeneration frees up glucose carbons for biomass diversion, and relieves lactate dehydrogenase of shouldering the burden of NAD regeneration on its own. Taken together with the studies described in Chapter 2, which show that LDH inhibition increases glucose consumption in Jurkat cells, our data point to a major role for glutamine and MDH1 in replenishing the NAD required for glycolysis reveal a potentially valuable therapeutic opportunity (Figure 3-4b). The dependence on, and increased consumption of, glutamine also revealed another potential vulnerability in cancer cells that captured our interest. Glutamine metabolism via the reductive carboxylation route occurs when the concentration of αKG in the mitochondria increases and is higher than citrate, one of the most abundant metabolites in the cell (Fendt et al., 2013b). Concentrations of αKG this high in the cell have other profound effects on proliferation as αKG can affect gene expression

through co-factor activity. Mutations in isocitrate dehydrogenase, the enzyme that produces αKG, are believed to be oncogenic drivers in glioblastomas and myeloid leukemias. Other studies have reported that increased concentrations of cellular αKG decrease proliferative potential and drive differentiation (Carey et al., 2015; Tennant and Gottlieb, 2010). In the following chapters, we explore the idea that elevated concentrations of the metabolite αKG affect cell growth, proliferation and survival by regulating gene expression.

Chapter 4

Resistance to chronic αKG treatment

Introduction

Cancer metabolism, at its surface is a reactive adaptation to the demands of cell division. The impetus for metabolic change is the up-regulation of proliferative pathways that call for diversion of carbon sources into the *de novo* generation of biomass. However, it is becoming increasingly clear that metabolites on their own have signaling capacity that can influence the physiology of a cell, including its proliferative potential. Since the potential to successfully perform cell division is closely tied to nutrient availability, it is not surprising that metabolites have evolved the ability to relay signals to the rest of the cell. Nutrient concentrations signal to the cell nutrient availability as well as the capacity for consumption. Our findings, showing that glutaminolysis and glutamine carbons support and regulate glucose consumption, are linked to this idea and served as a starting point for the studies described in this chapter (Hanse et al., 2017).

Inputs from both glucose and glutamine carbon intersect at alpha-ketoglutarate (αKG) in the TCA cycle (Figure 1-2), making accumulation of this metabolite a critical indicator of nutrient availability. Moreover, αKG is positioned early in the TCA cycle where accumulation could also signal decreased mitochondrial function or a decreased demand for electron transport. The cellular concentration of αKG could thus serve as a 'messenger', signaling metabolic fitness to the rest of the cell.

This message is relayed through an enzymatic co-factor function of αKG that is independent of metabolism. αKG binds to the active sites of DNA and histone demethylases and potentiates their activity. The removal of methylation moieties from cytosines within gene promoter regions can regulate access of RNA polymerase and influence gene expression (reviewed in (Fazzari and Greally, 2004)).

The importance of αKG in epigenetic regulation, particularly in the context of cancer became evident when it was discovered that glioblastomas and myeloid cell leukemias harbor mutations in isocitrate dehydrogenase (IDH), the enzyme that produces αKG from isocitrate. Specific mutations in the active site of IDH cause an incomplete reaction that results in the production of 2-hydroxyglutarate (2-HG), a metabolite that resembles αKG but is not readily metabolized in the cell. The accumulation of 2-HG was found to be oncogenic in that it represses differentiation and promotes stem like qualities (Figueroa et al., 2010; Losman et al., 2013; Lu et al., 2012). The oncogenic nature of 2-HG is manifest through competitive inhibition of αKG's co-factor function at these histone and cytosine demethylases.

If 2-HG is an oncogenic metabolite that functions through competitive inhibition of αKG, we reasoned that αKG accumulation could have tumor suppressive effects. Little is known regarding the specificity of genes or gene networks regulated by αKG dependent methyltransferases. Most studies have looked at global physiologic responses to αKG rather than its regulation of specific genes. We predict that αKG regulated gene responses are targeted and regulated, as indiscriminate, global, DNA/histone demethylation would be catastrophic to cancer cells.

We set out to identify specific genes and gene networks affected by αKG accumulation in cancer cells, predicting that these findings would offer a better understanding of the pathways involved in 2-HG dependent cancers, such as glioblastomas and myeloid leukemias. These findings could also potentially inform novel therapies targeted at αKG related pathways in a variety of cancers.

Results

Clonal Jurkat cells display a spectrum of sensitivities to αKG.

We evaluated the response of clonal lines derived from a heterogenous parental population of Jurkat human T leukemia cells to cell permeable (dimethyl) αKG (DM-αKG), and found a wide spectrum of sensitivities within the Jurkat population (Figure 4-1a). We asked whether the αKG sensitivity in clone 3 was a result of metabolic catastrophe or a reflection of the non-metabolic functions of αKG. To distinguish between the two possibilities, we attempted to rescue cell death with 2-hydroxyglutarate, an analog of αKG that functions as a competitive inhibitor of αKG rather than a metabolite. Sensitive clone 3 cells were rescued from cell death in a

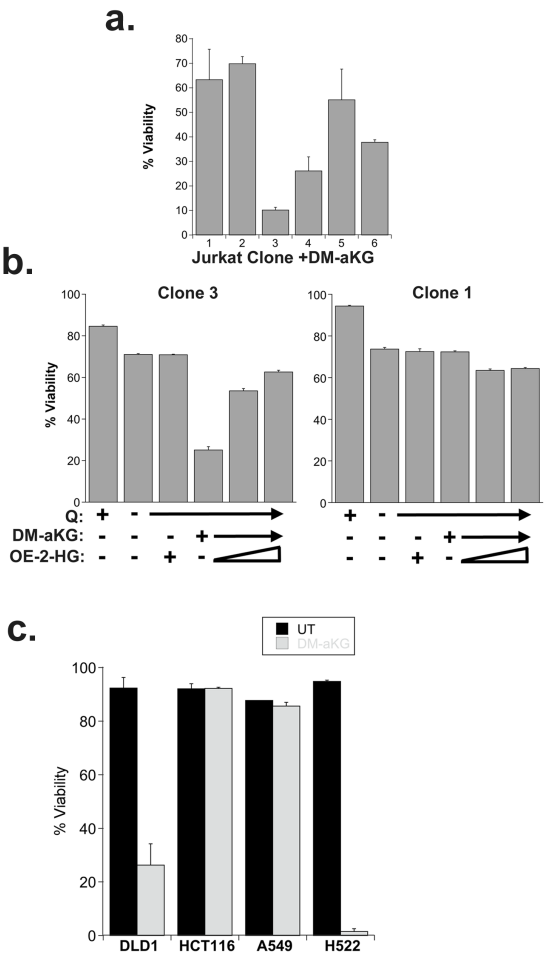

Figure 4-1. Varying sensitivities to α-ketoglutarate in cancer cells. Jurkat cells were single cell cloned and treated with 4mM αKG in the absence of glutamine for 24 hours. Shown is the viability as assayed by the annexin-V/propidium iodide death assay (a). Clone 3 (αKG sensitive) and Clone 1 (αKG resistant) were treated with αKG as in (a) and rescued with cell permeable octyl ester 2-hydroxyglutarate (OE-2-HG) (b). Human colorectal cell lines (DLD1, HCT116) and human lung cancer cell lines (A549, H522) were treated with 4mM αKG in the absence of glutamine for 24 hours. Viability was assayed via trypan blue exclusion (c).

dose dependent manner by the addition of 2-HG, suggesting that αKG was inducing cell death through mechanisms independent of metabolism (Figure 4-1b). We then tested commonly studied colorectal and lung cancer lines for their response to αKG and found variable sensitivities in these models as well (Figure 4-1c).

A high throughput screen to identify changes in the proteome brought about by chronic αKG treatment.

Little is known about the global effect on gene expression induced by persistently high levels of αKG concentration. To better understand the physiological effects of αKG treatment, we designed a high-throughput experiment to compare the proteomes of cells that were sensitive or resistant to αKG. We chose chronic treatment over acute as the pathways up-regulated after longer periods of time would be stable and more significant for survival in the presence of αKG.

We used Jurkat parental cells, which harbor a mixture of αKG sensitive and resistant cells (Figure 4-1a). We cultured the initial Jurkat parental cells in medium containing 4mM DM-αKG until a population emerged that proliferated at a comparable rate to untreated cells (approximately 30 days, data not shown). We followed this with a mass spectrometry based quantitative proteomics method, iTRAQ (Wiese et al., 2007), that compared the proteome of αKG resistant cells to that of the parental population, maintained in culture in parallel (Figure 4-2a). This method labels peptides with mass addition "barcodes" that allow analysis software to assign sample of origin from a mixture of samples (Figure 4-2a). Using both Protein Pilot and MaxQuant analysis software, we generated a list of over 1,000 significantly regulated proteins in αKG resistant cells (See Materials and Methods chapter for more details). The heat map for the most significantly regulated proteins using a maximum threshold for peptide identification is shown in Figure 4-2b. We also generated a list of the 'most regulated' proteins using less stringent exclusion criteria for peptide identification (Figure 4-3a). One of the most up-

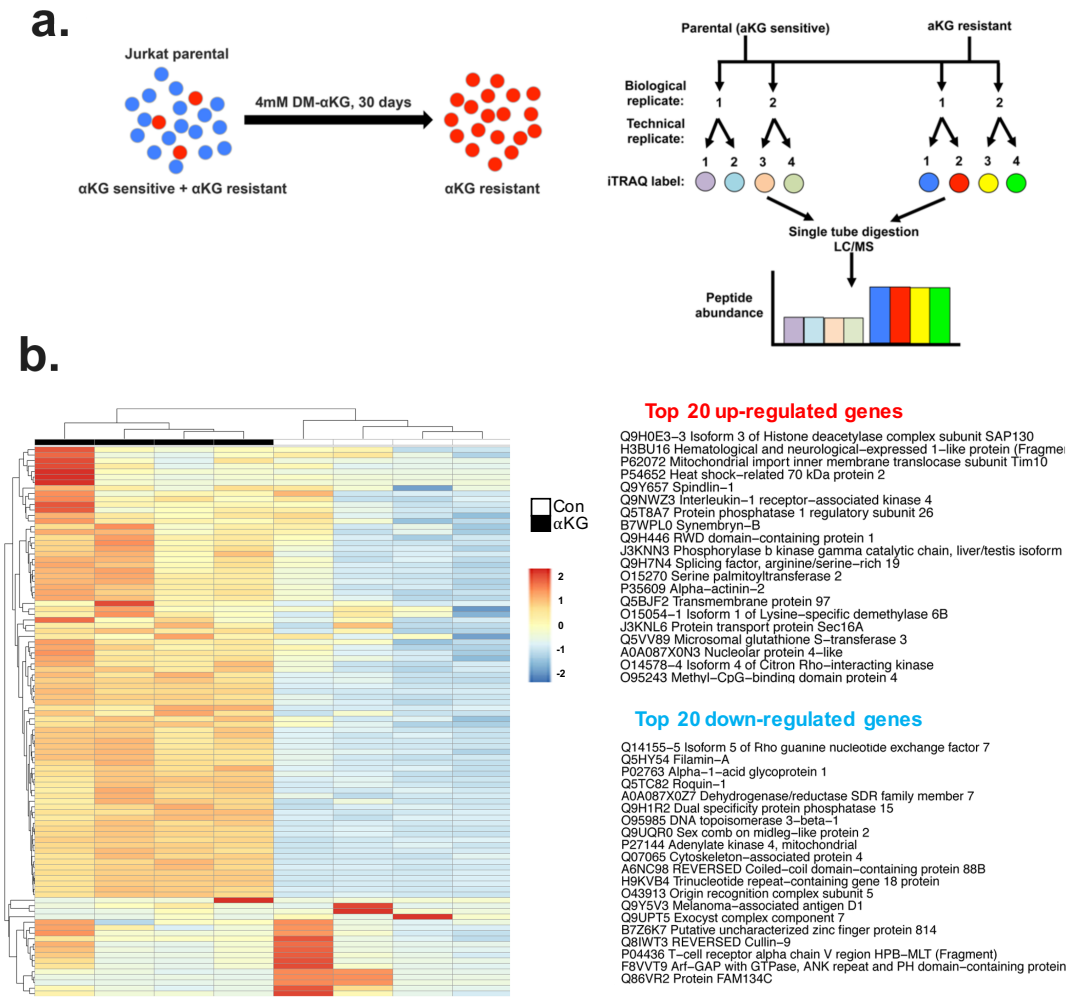

Figure 4-2. Chronic treatment with αKG causes significant changes to the proteome of Jurkat Cells. Schematic representing the generation of an αKG resistant population following chronic treatment (a, left). Schematic of the iTRAQ proteomics screen used to identify characterize the proteome of parental and αKG resistant cells (a, right). Heat map indicating the 100 most regulated proteins identified from iTRAQ via ProteinPilot software using a list generated from peptides with a high identification significance threshold ($p<0.001$).

regulated proteins in αKG resistant cells was citrate synthase (Figure 4-3a). To validate the iTRAQ screen, we single cell cloned the αKG resistant population by limit dilution and performed Western blot for citrate synthase. We found that almost all αKG resistant clones we tested had significantly increased citrate synthase

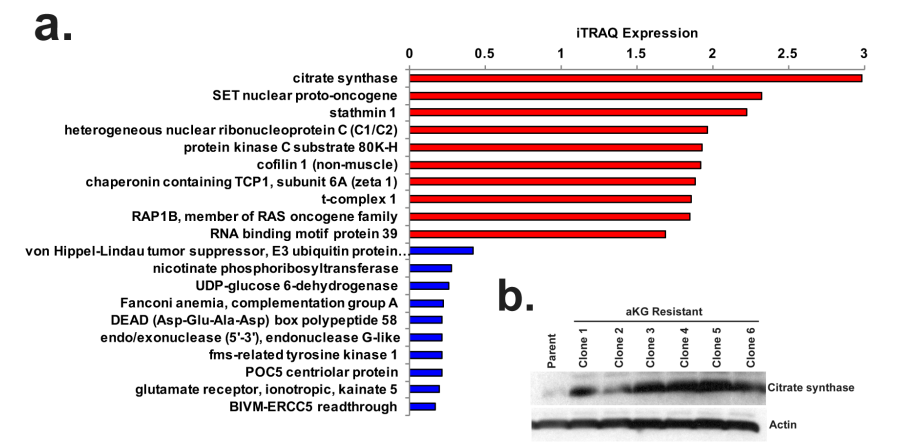
a.
iTRAQ Expression
0
0.5
1
1.5
2
2.5
3
citrate synthase
SET nuclear proto-oncogene
stathmin 1
heterogeneous nuclear ribonucleoprotein C (C1/C2)
protein kinase C substrate 80K-H
cofilin 1 (non-muscle)
chaperonin containing TCP1, subunit 6A (zeta 1)
t-complex 1
RAP1B, member of RAS oncogene family
RNA binding motif protein 39
von Hippel-Lindau tumor suppressor, E3 ubiquitin protein...
nicotinate phosphoribosyltransferase
UDP-glucose 6-dehydrogenase
Fanconi anemia, complementation group A
DEAD (Asp-Glu-Ala-Asp) box polypeptide 58
endo/exonuclease (5'-3'), endonuclease G-like
fms-related tyrosine kinase 1
POC5 centriolar protein
glutamate receptor, ionotropic, kainate 5
BIVM-ERCC5 readthrough
b.
aKG Resistant
Parent
Clone 1
Clone 2
Clone 3
Clone 4
Clone 5
Clone 6
Citrate synthase
Actin

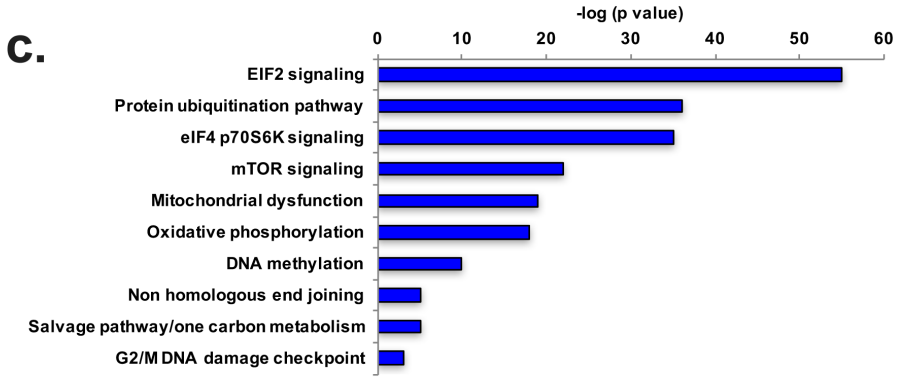
c.
-log (p value)
0
10
20
30
40
50
60
EIF2 signaling
Protein ubiquitination pathway
eIF4 p70S6K signaling
mTOR signaling
Mitochondrial dysfunction
Oxidative phosphorylation
DNA methylation
Non homologous end joining
Salvage pathway/one carbon metabolism
G2/M DNA damage checkpoint

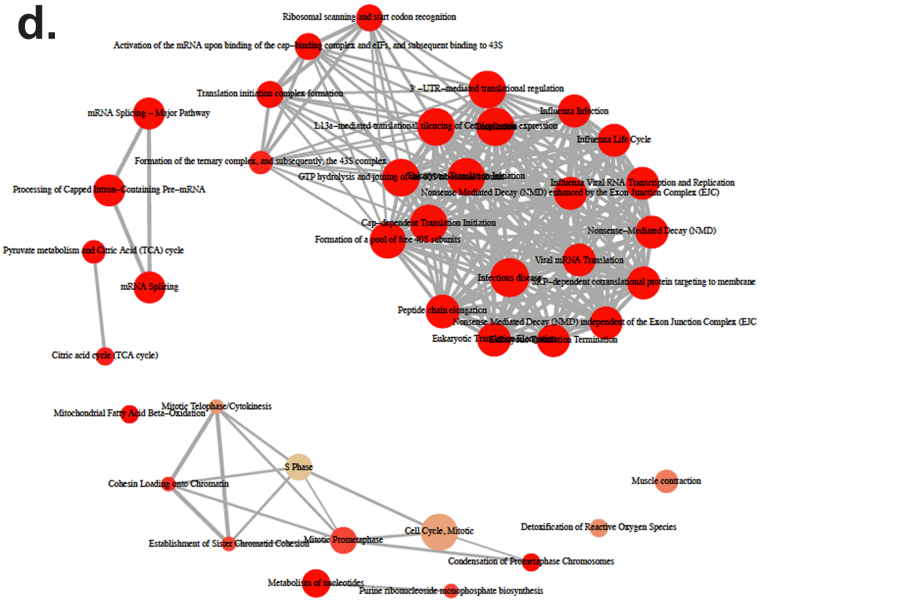
d.
Ribosomal scanning and start codon recognition
Activation of the mRNA upon binding of the cap-binding complex and eIFs, and subsequent binding to 43S
Translation initiation complex formation
5' -UTR-mediated translational regulation
mRNA Splicing - Major Pathway
L13a-mediated translational silencing of Ceruloplasmin expression
Influenza Infection
Influenza Life Cycle
Formation of the ternary complex, and subsequently, the 43S complex
GTP hydrolysis and joining of the 60S ribosomal subunit
Influenza Viral RNA Transcription and Replication
Nonsense Mediated Decay (NMD) enhanced by the Exon Junction Complex (EJC)
Processing of Capped Intron-Containing Pre-mRNA
Cap-dependent Translation Initiation
Formation of a pool of free 40S subunits
Nonsense-Mediated Decay (NMD)
Pyruvate metabolism and Citric Acid (TCA) cycle
Viral mRNA Translation
mRNA Splicing
SRP-dependent cotranslational protein targeting to membrane
Peptide chain elongation
Nonsense Mediated Decay (NMD) independent of the Exon Junction Complex (EJC
Eukaryotic Translation Elongation
Eukaryotic Translation Termination
Citric acid cycle (TCA cycle)
Mitotic Telophase/Cytokinesis
Mitochondrial Fatty Acid Beta-Oxidation
S Phase
Cohesin Loading onto Chromatin
Muscle contraction
Cell Cycle, Mitotic
Detoxification of Reactive Oxygen Species
Establishment of Sister Chromatid Cohesion
Mitotic Prometaphase
Condensation of Prometaphase Chromosomes
Metabolism of nucleotides
Purine ribonucleoside monophosphate biosynthesis

Figure 4-3. Pathway analyses of iTRAQ based proteomics in αKG resistant cells. List of most regulated proteins generated from a list positively identified peptides with no significance threshold (a). Western blot of Citrate Synthase from single cell clones derived from the αKG resistant population (b). Ingenuity Pathway Analysis from iTRAQ proteomics screen showing most significantly regulated pathways (c). Pathway networking analysis generated from Reactome software indicates strong network connectivity of translation initiation pathways (d).

protein expression compared to parental cells (Figure 4-3b). Citrate synthase (CS) precedes isocitrate dehydrogenase (that generates αKG from isocitrate) in the TCA cycle, catalyzing a reaction that synthesizes citrate from OAA and acetyl-CoA. The dramatic increase in CS protein expression was not expected. However, studies have shown that increased concentrations of αKG drive the reductive carboxylation of αKG toward citrate and out of the mitochondria. This directional push is dependent on the ratio of αKG to citrate in the cell (Fendt et al., 2013b). Up-regulating the expression of CS and, consequently, the capacity of the cell to generate citrate, could function as a mechanism of resistance to high αKG concentrations, driving the TCA back in the oxidative direction and the electron transport chain.

Proteomics pathway analysis reveals significantly altered pathways in αKG resistant cells.

To identify the most significantly regulated pathways in αKG resistant cells emerging from the iTRAQ screen, we analyzed the proteomics data using Ingenuity Pathway Analysis (IPA), Reactome and Perseus pathway analysis tools. The consensus results of the three analyses indicated that pathways involving the initiation of protein translation were the most significantly altered in αKG resistant cells and represented a novel and potentially significant mechanism of αKG influenced cell physiology (Figure 4-3c, 4-3d).

Conclusions

The proteomics screen provided valuable information about the impact of αKG on protein expression. On one hand the screen showed, as expected, that pathways such as oxidative phosphorylation, mitochondrial metabolism and the citric acid cycle were influenced by αKG. However, the screen also showed rather unexpectedly, that several protein translation pathways were altered in αKG resistant cells. One of the key regulators of protein translation, the mammalian target of rapamycin (mTOR), with its adaptor proteins that can sense amino acids such as leucine and directly signal to the protein translation apparatus the nutrient status of the cell, has often been implicated in cancer (Kim et al., 2002; Yuan et al., 2013). It is tempting to speculate that αKG has a similar role to play in regulating protein translation, perhaps through a parallel mechanism. The regulation of protein translation by αKG treatment is the focus of ongoing studies in the lab.

Our data also show significant regulation of One Carbon Metabolism (OCM) and DNA methylation pathways. These results were less surprising as the involvement of these pathways in 2-HG based oncogenesis has previously been reported (Koivunen et al., 2012; Koppenol et al., 2011). However, it was unclear how these pathways had adapted for survival in high αKG concentrations and we were interested in identifying the underlying mechanisms involved. This was a novel perspective that could provide deeper insight into the pathways cancer cells become dependent on during metabolic and/or epigenetic stress. We focused on these pathways for the next phase of our investigation.

Chapter 5

Targeting one carbon metabolism in αKG resistant cells

Introduction

The previous chapter described a high-throughput proteomics screen that revealed signaling pathways significantly impacted by chronic treatment with alpha-ketoglutarate (αKG). Among those most significantly up-regulated was one carbon metabolism (OCM) that produces methyl donors for methytransferase reactions. The methylation and demethylation of histones and cytosines directly affects gene expression. The OCM is thus an important pathway for maintaining the epigenetic landscape of cancer cells. OCM has been therapeutically targeted in a broad spectrum of tumors for decades, with drugs such as methotrexate and 5-fluorouracil that inhibit critical enzymes in this pathway reviewed in (Locasale, 2013).

We hypothesized that OCM was up-regulated in αKG resistant cells to counter the chronic demethylase activity induced by αKG ’s activation of Tet enzymes. Supporting this idea, a recent study indicated that colorectal and lung cancer cell lines, HCT116 and A549, harbor hyper-active OCM pathways (Maddocks et al., 2016). Interestingly, both these cell lines remained almost completely refractive to the death promoting effects of αKG (Chapter 4, Figure 4-1). In the following section, we explore the possibility that a hyperactive OCM, which underlies the resistance to αKG, exposes a vulnerability in the resistant cells that could be therapeutically exploited.

Results

At the outset, we studied the expression pattern of OCM pathway components that emerged from the iTRAQ proteomics screen described in the previous chapter. We found significant up-regulation of individual enzymes that make up the one carbon metabolism pathway, including the cytosine methyl-transferase DNMT1 (Figure 5-1a). We detected higher DNMT1 protein expression by Western blot in

nine different αKG resistant Jurkat clones compared to parental controls (Figure 5-1b).

a.

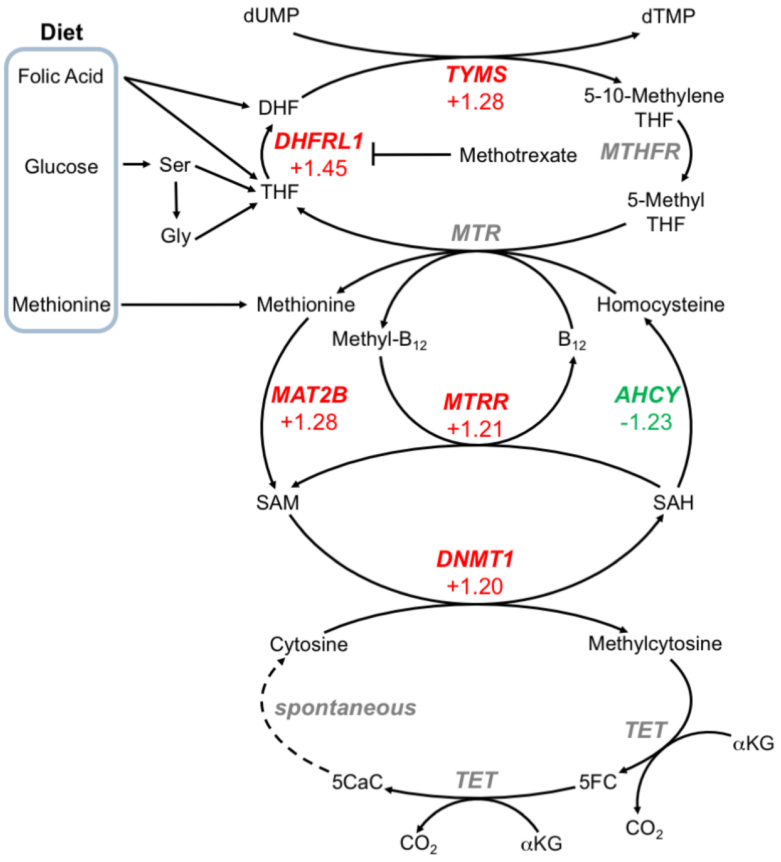

b.

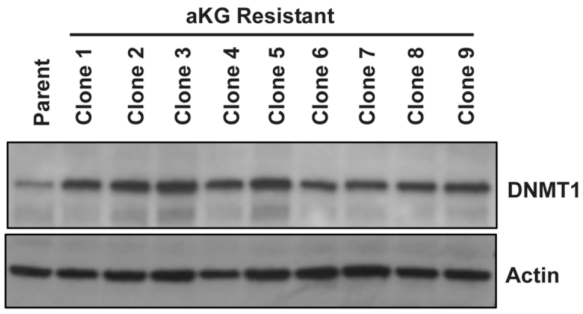

Figure 5-1. One carbon metabolism and the cytosine methylase DNMT1 are up-regulated in αKG resistant cells. The one carbon metabolism pathway that generates methyl donors from glucose, folate and methionine for cytosine methylation by DNMT1. Up-regulation is shown in red, down-regulation is shown in green with numbers indicating fold change in regulation relative to parental cells (a). Western blot of DNMT1 in αKG resistant clones (b).

As alluded to above, αKG 's activation of the Tet enzymes is predicted to cause changes in the epigenome. We hypothesized that OCM is enhanced as a counteractive measure aimed at restoring the methylation lost through the persistent Tet activity induced by αKG. Thus, inhibiting OCM could render these cells susceptible to αKG exposure. The DNMT inhibitor, decitabine (DAC), currently used in the clinic to treat myelodysplastic syndrome, has been gaining recognition for its therapeutic potential against a broad spectrum of cancers (Cashen et al., 2010; Karahoca and Momparler, 2013). The *in vitro* efficacy reported for DAC is in the 500nM range (Karahoca and Momparler, 2013; Turcan et al., 2013). A Phase II clinical trial for acute myeloid leukemia recorded a 29% response rate, with responsive patients showing DAC plasma concentrations of greater than 1uM. DAC has side effects, such as fatigue, nausea, significant reduction in white blood cell counts and susceptibility to infection. We asked whether the αKG resistant Jurkat cells (T cell acute lymphoid leukemia) were dependent on DNMT1 activity for survival and, consequently, sensitive to lower concentrations of DAC in the presence of αKG.

We found that αKG resistant Jurkat cells were susceptible to 1uM DAC in the absence of αKG (data not shown). However, two of the three αKG resistant clones tested were sensitive to concentrations of DAC as low as 10nm in the presence of 4mM αKG, whereas a third clone (Clone 3) continued to be resistant (Figure 5-2a). These results support our hypothesis that up-regulation of DNMT1 and increased dependence on the OCM is one mechanism of resistance to the αKG promoted enhanced demethylation. Our iTRAQ proteomics screen revealed several pathways significantly regulated by αKG treatment, and the persistent lack of

sensitivity exhibited by Clone 3 to αKG in the presence of DAC suggests that alternative mechanisms of αKG resistance might be in play in this clone. This will require further investigation in the future.

We next looked at the colorectal (HCT116) and lung (A549) cancer cell lines, reported to show increased dependence on OCM (Maddocks et al., 2016), that we had determined were resistant to αKG (Figure 4-1). Again, both cell lines exhibited significant sensitivity to nanomolar concentrations of DAC in the presence of 4mM αKG (Figure 5-2b). We conclude from these data that αKG -induced persistent activation of the TET family of cytosine demethylases can lead to tumor suppressive changes to the epigenetic landscape, unless countered by constitutive activation of OCM or up-regulation of DNMT1 activity aimed at restoring the methylation patterns and repressive gene signatures of the cancer genome. This dependence on OCM exposes a vulnerability and opens a therapeutic window that can be exploited by OCM or DNMT1 inhibitors, such as DAC.

Discussion

The results described here identify one plausible mechanism for decreased sensitivity to increased intracellular concentrations of αKG observed in some cancers. We had hypothesized that αKG could function as a tumor suppressor metabolite, based on the oncogenic properties of its antagonist 2HG (see Chapter 1). The studies described in Chapters 4 and 5 support this characterization of αKG. Furthermore, our iTRAQ data offer a platform to begin identifying the fundamental mechanisms that may be harnessed for survival in the presence of this natural tumor suppressor. Although our current studies are limited to studying the effects of exogenously added cell permeable αKG, future studies will focus on evaluating DAC sensitivity in cells that are highly dependent on glutamine, such as Myc driven cancers. We are also interested in increasing intracellular αKG levels

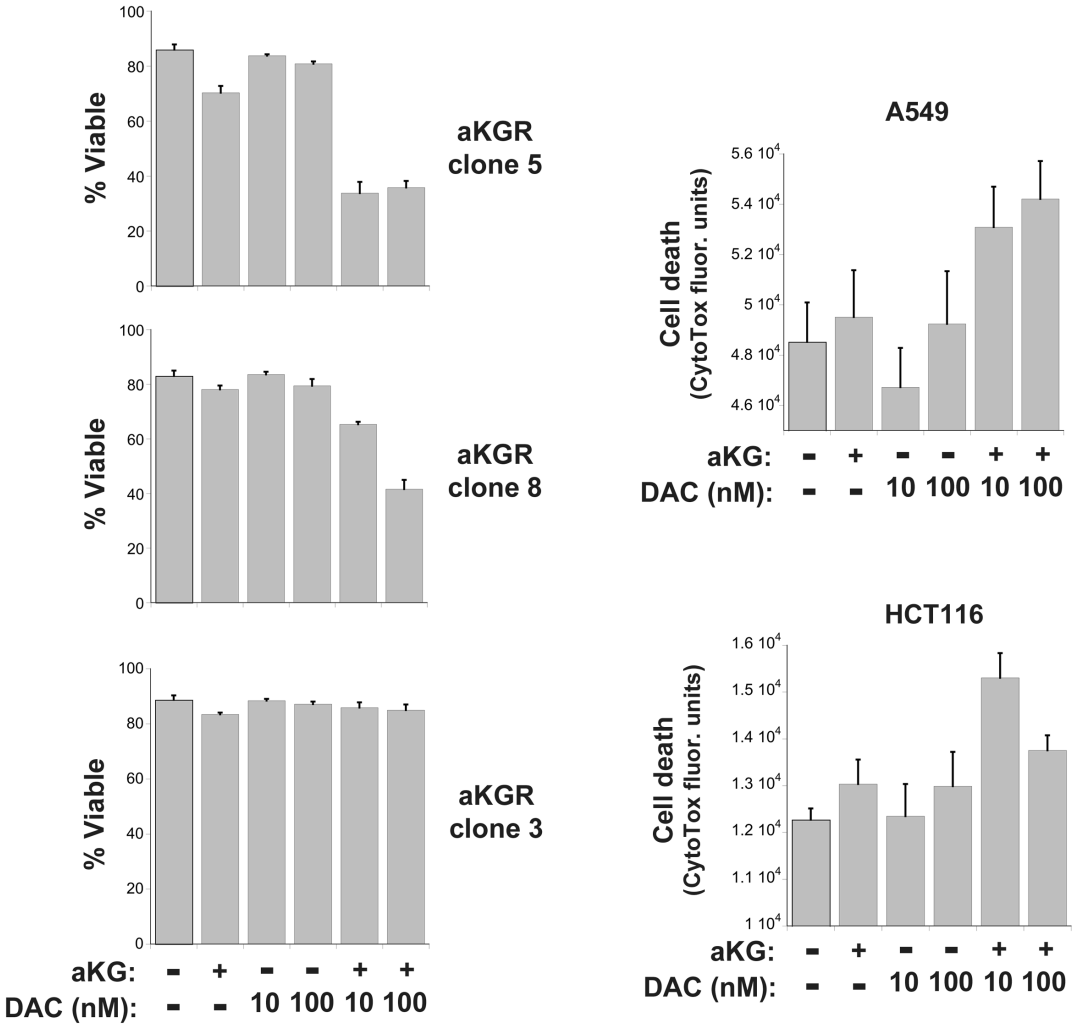

Figure 5-2. Treatment with αKG sensitizes cancer cells to the DNMT1 inhibitor decitabine. Cell viability assayed by annexin-V/propidium iodide staining in αKG resistant clones (aKGR) derived from the population of cells used for the iTRAQ proteomics screen (a). Cell death in human lung (A549) and colorectal (HCT116) cancer cell lines assayed by cytotoxicity fluorescence (b).

pharmacologically by limiting oxidative phosphorylation with metformin (Wheaton et al., 2014) or low dose oligomycin (Sullivan et al., 2015). These data also support our hypothesis that cancer cells counter the growth suppressive effects of increased TET demethylase activity resulting from increased αKG concentrations

by activating the pathway that provides methyl donors, including the methyl-transferase itself.

This would constitute a novel, 2-HG independent mechanism for repressing the downstream consequences of enhanced co-factor activity of αKG. Isocitrate dehydrogenase mutations have been reported primarily in glioblastomas and acute myeloid leukemias. However, many cancer cell types are dependent on increased glutamine consumption and are likely to have acquired adaptations to resist the effects of accumulation of this tumor suppressor metabolite and, as observed in clone 3 (Figure 5-2), these adaptations may not be restricted to OCM upregulation.

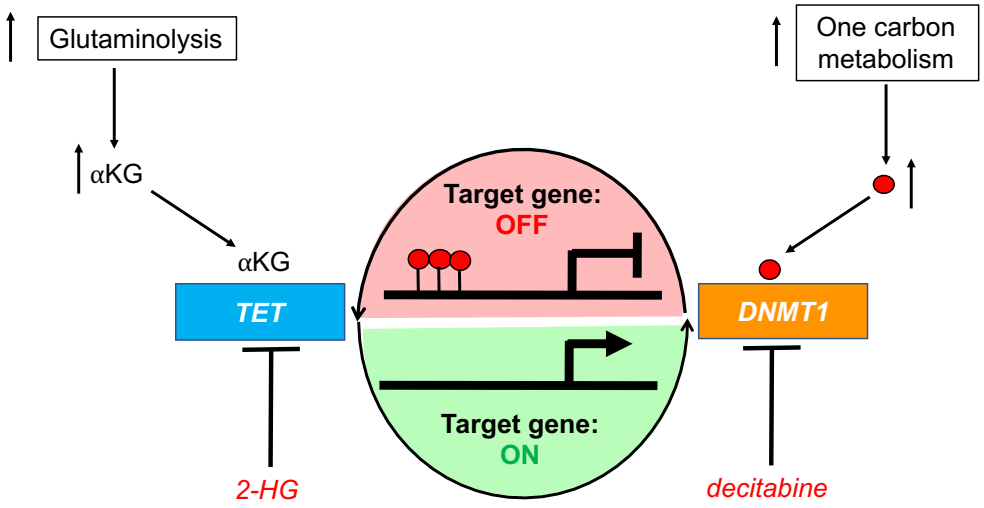

Figure 5-3. Model of the epigenetic methylation cycle. Increased cellular concentrations of αKG activate TET demethylases which, in turn remove inhibitory methyl groups (red circles) from the promoters of target genes and activate gene expression. Tet activity is inhibited by 2-HG in glioblastomas and myeloid leukemias. Up-regulation of the one carbon metabolism pathway and over-expression of DNMT1 restores promoter methylation and represses target gene expression. Our results suggest decitabine may be an effective therapeutic in cells with increased intracellular αKG concentrations.

By revealing a dependence on one carbon metabolism and DNMT1, our studies expose a therapeutic window in a potentially broad panel of cancers. This increased dependence on DNMT1 is highly significant. Given its high plasma concentrations in responsive patients and its side effect profiles, the DNMT1 inhibitor decitabine has yet to be adopted as an acceptable alternative to harsher chemotherapies or bone marrow transplants. However, our data show that decitabine is effective at killing αKG treated cells with concentrations two orders of magnitude lower than previously reported. These results could provide valuable insight into the efficacy of this drug in treating glutamine addicted tumors. Our studies also lay the foundation for the development of an αKG based treatment for cancer, specifically in combination with inhibitors of one carbon metabolism or methyltransferases.

Chapter 6
Discussion and future directions

Discussion and Future Directions

The studies described here are centered around the metabolism of cancer. The profound metabolic changes that occur during proliferation can both be the cause and effect of tumorigenesis. Our studies bring significant new knowledge to both aspects of tumor metabolism that will inform the future of targeted therapies.

We demonstrate that the Warburg effect, thought to be dependent solely on lactate dehydrogenase, utilizes malate dehydrogenase 1 (MDH1) as the cytosolic NAD regeneration mechanism. We report *MDH1* is amplified more often than *LDH* and correlates with poor patient prognosis. These are important findings as therapies targeting lactate dehydrogenase are entering clinical trials (Augoff et al., 2015; Billiard et al., 2013; Rani and Kumar, 2016). We argue that MDH1 will also need to be targeted to effectively limit glucose consumption and the utilization of glucose carbon for biomass generation. Our results suggest MDH1 may even be a more 'efficient' source for NAD in the cytosol than LDH. We report that in the presence of MDH1, LDHA inhibition *increased* glucose consumption. Quantitatively it makes little sense to compare malate and lactate flux in the cell since lactate, as an endpoint metabolite tends to accumulate, unlike malate which is transient and acts as substrate for several other reactions. This is an important distinction. Malate, in addition to functioning as an NAD regenerator, could also serve as a contributor to biomass as a substrate for the synthesis of non-essential amino acids or pyruvate. An independent published study found that pancreatic ductal carcinomas overexpress MDH1 to generate malate for malic enzyme which produces the NADPH required to quell the high oxidative stress of proliferation (Wang et al., 2016). In the cell types that we looked at, we found LDHA inhibition to have minimal effect on proliferation, in contrast to studies that had shown LDHA inhibition to be effective at inhibiting tumor cell growth (Billiard et al., 2013; Xie et al., 2014). Although our data conflict with these studies, there are studies suggesting lactate secretion and re-uptake may play a critical role in maintaining

de-differentiation by signaling in the NF-KB pathway (Vegran et al., 2011). It has been suggested, moreover, that in animal models, increased lactate in the tumor microenvironment can stimulate endothelial cells to increase angiogenesis (Sonveaux et al., 2012). It is important to note that our studies, rather than minimizing the value of lactate in cancer metabolism, are pointing to a novel supporting role for MDH1 providing, thereby, a more comprehensive view of Warburg metabolism. While the utility of lactate could wax and wane during tumorigenesis, increased glycolysis, and increased carbon appetite for biomass are constants during proliferation, underscoring the importance of targeting both dehydrogenases throughout tumor development.

To date, attention has been focused largely on the TCA cycle mitochondrial enzyme, malate dehydrogenase 2 (MDH2), and little is known about the structure of MDH1. Ongoing studies to address this lacuna include collaborative efforts with the Department of Medicinal Chemistry at the University of Minnesota to crystallize MDH1 and solve its structure, as well as computer modeling to create a “smart” library of compounds and set up a high throughput assay to screen for MDH1 specific inhibitors.

Our studies suggest that glutamine is a carbon source for the MDH1 reaction. Although, it is unlikely to be the only carbon source for this enzyme, we demonstrate that the availability of glutamine for the MDH1 reaction correlates with increased glycolysis. Indeed, we found dependence on glutamine for proliferation and glucose consumption is tied to MDH1 status again highlighting the importance of this reaction. To our knowledge, this is the first study showing how glutamine carbons are essential for supporting glycolysis. The linking of these two carbon sources through MDH1 reveals a metabolic vulnerability in cancer cells.

Our studies also describe how cancer metabolism affects proliferation. The increased glutamine consumption by proliferating cells is often coupled with

increased intracellular concentrations of αKG. The αKG in turn acts on a variety of non-metabolic enzymes that regulate gene expression. We offer evidence to support our hypothesis that αKG can function as a tumor suppressor and reveal novel pathways affected by αKG treatment. This is a newer concept in the field but is proving to be important in understanding how metabolism is woven into the physiology of the entire cell. The relaying of messages conveying nutrient availability is not by itself a novel idea. However, the messenger metabolites involved in relaying these signals and the mechanisms activated in response, to implement the required changes, are not fully understood. The realization that 2-HG, the αKG antagonist, is a potent driver of oncogenesis has brought into focus the pathways affected by αKG. The increased intracellular concentrations of αKG precipitated by increased glutamine uptake, or perhaps through therapeutic intervention, are beginning to reveal vulnerabilities in tumor metabolism not previously appreciated. We utilized an innovative proteomics approach to parse out the most important pathways required for survival in cancer cells chronically exposed to αKG. The pathways revealed in our study open new and exciting avenues for future research. For example, the most significantly regulated pathways from both Ingenuity and Reactome pathway analyses involved initiation of protein translation. Further analyses of these pathways using Reactome, clustered these pathways in a manner that predicts mammalian target of rapamycin (mTOR) the master regulator of protein translation, as being fundamentally associated with αKG regulated protein translation. On its own, mTOR is one of the most investigated kinases in cancer metabolism today (Zoncu et al., 2011). Thus, the idea of mTOR as a sensor of input signals from nutrients is not new. Other groups have shown non-essential amino acids signal to mTOR through adaptor proteins that help initiate cellular protein translation or induce autophagy based on supply and demand (Kim et al., 2002; Kim et al., 2011). Surprisingly, αKG is yet to be implicated in any of these studies and future investigation in the lab will focus on this association.

Another major pathway affected by αKG treatment that emerged in our analysis was DNA methylation through one carbon metabolism. This pathway became the focus of our follow up studies for two reasons. First, αKG is a co-factor for the Tet family of enzymes that de-methylate cytosines and this activity is reported to be one of the crucial enzymatic mechanisms targeted by 2-HG during transformation (Xu et al., 2011). Thus, the one carbon metabolism pathway, constitutively activated for restoring methylation status, is an attractive target for therapeutic intervention in combination with αKG. Second, one carbon metabolism has been the focus of intense study and chemotherapeutics for decades. For example, methotrexate a DHFRL1 inhibitor, is a first line leukemia drug and 5-fluoruracil, used as therapeutic in many cancers is a semi-selective inhibitor of DNMT1. Although the epigenetics of a tumor cell change over time, it is becoming increasingly clear that acute changes to methylation can be catastrophic and induce cell death. Thus, we may have identified a new strategy whereby clinically approved drugs targeting one carbon metabolism could be combined with αKG to potentiate tumor death at lower dosages, minimizing off target side effects and improving quality of life. Indeed, combination of αKG treatment with the specific DNMT1 inhibitor decitabine reduced the amounts of drug required to promote death by at least one hundred-fold. Our findings suggest that, in combination with αKG, the use of decitiabine, already available in the clinic for treating some leukemias could be expanded to treat other tumor types.

Many more questions about the nature of αKG induced cytosine demethylation remain unanswered. Previous studies have reported treatment of pluripotent stem cells with αKG induces differentiation through global epigenetic changes (Figueroa et al., 2010; Losman et al., 2013; Lu et al., 2012). Importantly, αKG treatment has not been reported to demethylate cytosines with any specificity. Our hypothesis that αKG acts as a signaling metabolite to relay messages and influence physiology, encompasses the idea that αKG induced TET activity is directed at specific genes. We have performed some preliminary studies using methyl DNA

immunoprecipitation (MeDIP) to further test this idea. Preliminary studies strongly suggest that αKG induced promoter demethylation is specifically targeted (data not shown). These studies are ongoing and we anticipate identifying a library of promoters demethylated by αKG treatment in the future. This information will be valuable for developing therapeutic strategies centered around this natural tumor suppressor metabolite.

In conclusion, these studies have made novel and significant advances in our understanding of metabolism in cancer, focusing not only on how proliferation affects metabolism but also on how metabolism affects proliferation. Our results inform a diverse audience of cancer researchers and are relevant to a large variety of tumors. These findings could lead to new cancer therapies that build upon current strategies based on how cancer cells utilize carbon. Our findings also lay the foundation for novel therapeutic approaches that can be applied to a broad field of proliferative diseases.

Chapter 7

Materials and methods

Cell Culture

Jurkat, HL60, DLD1, H522 and K562 (ATCC) cells were maintained in RPMI-1640 medium supplemented with 10% FBS, 100 U/ml penicillin, 100ug/ml streptomycin, NEAA, and 4mM L-glutamine. HEK293, A549, HCT116 and HeLa (ATCC) cells were maintained in DMEM supplemented with 10% FBS, 100 U/ml penicillin and 100ug/ml streptomycin. JPar and N5 cells have been previously described (Lowman). MDH1 KO cells were a generous gift from Kivanc Birsoy and David Sabatini. The LDHA inhibitor, GSK 2837808A (Tocris Bioscience, Bristol UK) was solubilized in DMSO, added to culture medium at the time of plating and maintained at 10uM throughout the experiment. Decitabine was purchased from Selleckchem (Houston, TX USA) dissolved in DMSO and used at indicated concentrations.

Glucose and Lactate Measurements

Concentration of glucose in the medium was measured via the EnzyChrom Glucose Assay Kit (BioAssay Systems, Hayward, CA USA) according to the manufacturer's protocol, and then normalized to cell counts. Concentration of lactate in the medium was measured via the Lactate Assay kit (Sigma-Aldrich, St. Louis, MO USA) following filtration through a 10,000Kd MWCO spin filter. Lactate measurements were then normalized to cell number.

Plasmid Constructs

The MDH1 plasmid was a kind gift from S.M. Lee (Lee et al., 2009). The MDH1 insert was amplified from the source vector to carry a 5' FLAG tag and cloned into pcDNA 3.1 and verified by sequencing. The pcDNA 3.1 lacZ Myc/His construct was used as a vector control. Transfections were carried out in 5E6 cells A549 cells using 1ug of plasmid and 5ul of FuGENE HD (Promega, Madison, WI USA) reagent in 200ul of antibiotic free medium. After a 15-minute incubation at ambient temperature, the DNA/FuGENE complex was added to a sub-confluent 10cm plate containing 10ml of antibiotic free medium. After 24 hours of transfection, medium

was replaced and supplemented with 1mg/ml of G418 (Geneticin) for one week. For Jurkat transfections, 10ug of plasmid was electroporated using a Neon Transfection System (Invitrogen, Carlsbad, CA, USA) into 10E6 cells in a 100ul Neon tip using 1350V at a pulse width of 10ms for 3 pulses. Cells were returned to antibiotic free medium for 24 hours. After 24 hours, medium was supplemented with G418 for 10 days. Live cells were recovered using a Ficoll density gradient.

Western Blot

Cells were washed 1X with cold PBS, resuspended in Radio immunoprecipitation (RIPA) buffer supplemented with protease and phosphatase inhibitor cocktails. Lysates were incubated on ice for 10 min and spun at 10,000 rpm at 4°C in a microcentrifuge. The supernatant was collected for further analysis. After BCA protein assay, equal amounts of protein (10-50µg) were resolved by SDS-PAGE, transferred to nitrocellulose and probed with antibodies specific for Noxa (Santa Cruz, Santa Cruz, CA USA; SC-56169), beta actin (Santa Cruz; SC-69879), MDH1 (Abcam, Cambridge, MA USA; Ab180152), LDHA (Cell Signaling Technology, Danvers, MA USA; #3582) Citrate synthase (Thermo Scientific, Rockford, IL; #GT2061) DNMT1 (Cell Signaling Technology; #5032) or the FLAG epitope (Sigma-Aldrich, St. Louis, MO USA; F7425).

Seahorse Extracellular Flux Assay

Seahorse base medium (Agilent, Santa Clara, CA USA) was supplemented with 10mM glucose, 1mM sodium pyruvate and 4mM L-glutamine and adjusted to pH 7.4 with NaOH. Cells were plated at 250,000 cells per well and adhered to the Seahorse 96 well culture plate using CellTak (Corning, Oneonta, NY USA). Extracellular acidification rate (ECAR) and oxygen consumption rate (OCR) were measured using the Seahorse XFe96 (Agilent, Santa Clara, CA USA).

Metabolic labeling experiments in cell culture

Live, healthy cells were recovered by Ficoll density gradient centrifugation within 24 hours prior to experiment. At T_0 10E6-20E6 cells per sample were pelleted and washed in glucose/glutamine free medium. For glucose labeling experiments, cells were resuspended at 1E6 cells/ml in complete glucose free medium supplemented with 10% dialyzed FBS, NEAA, and 4mM L-glutamine for 1 hour. After starvation, cells were supplemented with 10mM [^{13}C] or [^{2}H] labeled glucose for the time indicated in each experiment. For glutamine labeling experiments cells were washed and then resuspended in complete glutamine free medium supplemented with 10% dialyzed FBS and 10mM glucose for 3-4 hours. Following depravation, 4mM [U-^{13}C] glutamine was added to the medium and cells were incubated for 24 hours. Cells were then pelleted and washed 1X in ice cold PBS. Pellets were then resuspended in 100-200µl -20°C methanol, snap frozen and stored at -80C. Liquid chromatography/mass spectrometry (LC/MS) and gas chromatography/mass spectrometry (GC/MS) were used for identification and quantification of labeled metabolites of all samples. [1,2-^{13}C] glucose and [U-^{13}C] glutamine was purchased from Cambridge Isotopes (Tewksbury, MA USA) and [4-^{2}H] glucose was purchased from Omicron Biochemicals (South Bend, IN USA).

Primary T cell experiments

Human peripheral blood mononuclear cells (PBMCs) were obtained from a healthy donor via Memorial Blood Center (St. Paul, MN USA). PBMCs were purified from red blood cells using Histopaque. CD3+ T cells were isolated from PBMCs using the negative selection MACS magnetic separation system (Miltenyi Biotec, San Diego, CA USA) and allowed to recover in RPMI-1640 supplemented with 10% FBS, 100 U/ml penicillin, 100µg/ml streptomycin, NEAA, and 4mM L-glutamine overnight. At 18 hours, live T cells were recovered by Ficoll density gradient centrifugation and allowed to rest for 4 hours before being washed in glucose-free medium and starved of glucose for 1 hour. For activation and metabolic labeling, T cells were moved to culture dishes coated with 5µg/ml anti-CD3 antibody

(Biolegend, San Diego, CA USA). 5ug/ml of anti-CD-28 antibody (Biolegend) was then added along with 10mM [4-^{2}H] glucose. Cells were harvested 18 hours later, resuspended in 150µl of cold -20°C methanol, snap frozen and stored at -80°C until required for metabolomics analysis.

Central Carbon Metabolism sample preparation

Microtubes containing cell pellets were removed from -80°C storage and maintained on wet ice throughout the processing steps. To initiate protein precipitation, 0.3 mL of a chilled mixture of methanol, chloroform and water (8:1:1) (EMD) was added to each sample, the mixture vortexed briefly, and allowed to incubate on ice for 10 mins. Post-incubation, the vortex step was repeated, and samples centrifuged at 14,000 RPM, for 10 mins in 4°C. Post-centrifugation, 100 µL of supernatant was transferred to an autosampler vial for LC-MS analysis. From the remaining supernatant from each sample, a small aliquot was transferred to a new microtube to create a pooled sample for quality control purposes. The remaining supernatant from each sample was transferred to an autosampler vial, and brought to dryness. To each sample, 50 µL of 20 mg/mL of a solution of methoxyamine hydrochloride in pyridine was added. Samples were vortexed briefly and the samples incubated at 37°C for 90 mins. Samples were removed from heating and allowed to cool to room temperature. Addition of 50 µL of MTBSTFA with 1% tBDCMS (Regis Technologies, Morton Grove, IL USA) and samples were incubated at 70°C for one hour. Samples were cooled and GC-MS was performed. A series of calibration standards were prepared along with samples for quality control of instrument performance and chromatography for both LC and GC analysis.

LC-MS analysis

LC-MS analysis was performed on an Agilent system consisting of a 1260 UPLC module coupled with a 6520 Quadrupole-Time-of-flight (QTOF) mass spectrometer (Agilent Technologies, Santa Clara, CA USA) Metabolites were

separated on a 150x1mm Luna NH_2 hydrophilic interaction chromatography column (Phenomenex, Torrance, CA USA) using 10 mM ammonium acetate in water, adjusted to pH 9.9 with ammonium hydroxide, as mobile phase A, and acetonitrile as mobile phase B. The flow rate was 0.075 mL/min and the gradient was linear 20% to 100% A over 15 mins, followed by isocratic elution at 100% A for 5 minutes. The system was returned to starting conditions (20% A) in 0.1 min and held there for 10 minutes to allow for column re-equilibration before injecting another sample. The mass spectrometer was operated in ESI- mode according to previously published conditions (Lorenz et al., 2011).

GC-MS analysis

GC-MS analysis was performed on an Agilent 69890N GC -5975 MS detector with the following parameters: a 1µL sample was injected splitlessly on an HP-5MS 15m column (Agilent Technologies) with a helium gas flow rate of 1.4 mL/min. The GC oven initial temperature was 60°C and was increased at 10°C per minute to 300°C, and held at 300°C for 5 mins. The inlet temperature was 250°C and the MS-source and quad temperatures were 230°C and 150°C respectively.

Metabolite Data Analysis

For LC-MS analysis, metabolite peaks (both molecular ion and stable isotopes) were identified by matching the retention time and mass (+/- 10 ppm) to authentic standards. For GC-MS, metabolite peaks (both molecular ion and stable isotopes) were identified by matching the retention time and mass (+/- 0.2 Da) to authentic standards. Metabolite masses (M-H for LC-MS, TBDMS derivative for GC-MS) are indicated in Supplementary Table 1, along with the qualifying ions used for the GC-MS identification. Isotope peaks (natural abundance and stable isotope labeling) were identified as increments of +1.0034 Da and +1 Da, respectively. Presence of stable isotope labeling above the natural abundance was verified by absence of the same MS peak in the unlabeled preparation of the same condition. Peak areas were integrated using MassHunter Quantitative Analysis vB.07.00 (Agilent

Technologies) Peak areas were corrected for natural isotope abundance using an in-house written software package based on the method described previously (Lewis et al., 2014) and the residual isotope signal was reported. Data were normalized to cell protein content prior to analysis of metabolite fluxes for Central Carbon metabolites.

Soft Agar Colony Assays

Soft agar plates were prepared by mixing 3.2% low melt agarose with DMEM culture medium to yield 0.8% agarose at 38.5C. 1ml was added per well of a 6 well plate and allowed to solidify. 11,500 cells per ml were then mixed with 3.2% agarose to yield 0.48% agarose in DMEM culture medium and allowed to solidify. 1ml of DMEM supplemented with 1mg/ml G418 was added to the top of the agarose. Each condition was plated in triplicate. Plates were incubated for 15 days. Colonies were stained with 0.005% crystal violet in PBS and 4% formaldehyde. Images were captured on an inverted microscope using QCapture software. Ten microscopic fields were captured and counted per condition. Colonies were counted using ImageJ software.

Alpha-ketoglutarate cell viability assays

Pure dimethyl-αKG was added to culture medium at 4mM. Cells were incubated for indicated times. For suspension cells, cultures were pelleted and washed in PBS. Cell pellets were then resuspended in 400ul of Annexin V-FITC (Biovision) and propidium iodide (0.5ug/ml) and analyzed on the LSRII (BDF Bioscience). Untreated cells were used to identify live populations and percentage of cells in this quadrant were applied to all conditions. For adherent cells, cell viability was measured via trypan blue exclusion using the Vicell (Beckman Coulter, Indianapolis, IN USA) by combining spent medium, PBS wash and trypsinized cells into a single tube for counting. Cytotoxcity was measured using the CytoTox Fluor kit per manufacturer's instructions (Promega, Madison, WI USA).

Generation of alpha-ketoglutarate resistant cells

Jurkat parental cells (ATCC) were grown to confluence and split into two 10ml cultures. One culture was treated with 4mM DM-αKG, the other was untreated. At days 2, 4, 7, 11, 15, 18, 22, 26 fresh medium and DM-αKG was added. At day 31, cells were collected and frozen down in liquid nitrogen. Bulk populations were used for proteomics experiments. Bulk cells were single cell cloned by limit dilution, grown to confluence and frozen in liquid nitrogen.

iTRAQ proteomics of alpha-ketoglutarate resistant cells

Parental Jurkat controls and bulk KG resistant cells were split into duplicate cultures and allowed to grow with or without 4mM DM-αKG for 2 days. Cells were pelleted and washed with ice cold 50ml PBS 5 times. The final pellet was dried by careful aspiration and stored at -80˚C.

iTRAQ proteomics mass spectrometry

We performed second dimension liquid chromatography (LC) online with an Orbitrap Velos mass spectrometer (MS) system (ThermoFisher, Waltham MA) as previously described (Lin-Moshier et al., 2013). Minor modifications to the capillary LC and MS parameters were: HCD activation time was 20 milliseconds; lock mass was off; dynamic exclusion settings were: repeat count = 1, exclusion list size = 500, exclusion duration = 30 seconds, exclusion mass width (high and low) was 15 ppm and early expiration was disabled.

iTRAQ Proteomics Database Searching

We converted the raw MS datafiles to MGF files with MS Convert from ProteoWizard Toolkit (PMID: 23051804). We used ProteinPilot™ v5.0 (Sciex, Framingham, MA), which uses the Paragon™ scoring algorithm (Shilov et al., 2007) and the ProGroup™ protein grouping algorithm, for protein detection and relative quantification from peptide tandem MS data with MGF files as the input. We used the UniProt (http://www.uniprot.org/) human protein database from Dec

13, 2017 combined with the contaminants database (http://www.thegpm.org/cRAP/index.html) for a total of 92993 protein sequences as the reference database. ProteinPilot™ search parameters were: 8-plex peptide label sample type; cysteine methyl methanethiosulfonate; trypsin; instrument Orbi MS (1–3ppm) Orbi MS/MS; biological modifications ID focus; thorough search effort; detected protein threshold 0.05 (10%), competitive error margin 2.00 and false discovery rate analysis invoked (with reversed database). False discovery rate (FDR) calculations were performed in ProteinPilot™ with the concatenated forward and reversed protein sequence databases according to the method previously reported (Tang et al., 2008). ProteinPilot™ calculates an average protein relative fold change between two conditions along with a 95% confidence interval for the fold change and a p-value for a test of the null hypothesis unity (1:1 ratio), which helps assess the statistical significance of a fold change.

iTRAQ Proteomics Statistics and Pathway Analysis

For a set of samples, ProteinPilot tests each subsequent sample against the first sample in the dataset (in this case, a control sample), and gives a ratio of protein expression between each subsequent sample and the first sample, as well as a p-value for differential expression. Data were filtered to remove non-human, uncharacterized and cRAP proteins, as well as any proteins where any values were missing. To get a list of the proteins that were different between control and αKG samples, strict filtering criteria were used: Since values are all ratios of a sample's expression for a given protein compared to the first sample, proteins were only retained if the subsequent three control samples each had non-significant differences in expression, and the four αKG resistant samples had a significant difference. This limited the data to 230 proteins. A heatmap map of expression ratios was generated in R, using a value of 1 (it's ratio to itself) for the first sample (the sample which was the denominator in the expression ratios for all other samples). The R package ReactomePA (Yu and He, 2016)was used for pathway

analysis and to generate an enrichment map using the corresponding genes for the 230 significant proteins.

An additional data analysis survey was performed by using MaxQuant. Following Maxquant converstion, data were filtered and analyzed in Perseus (Tyanova et al., 2016), removing proteins only identified by site, reverse sequences and potential contaminants. Data were log2 transformed and further filtered to remove proteins with NA values in more than 4 samples. Two sample t-tests were conducted to determine significantly differentially expressed proteins. A Fisher's exact test was used to test for enrichment of GO terms, GSEA, KEGG and Reactome annotations.

Bibliography

Augoff, K., Hryniewicz-Jankowska, A., and Tabola, R. (2015). Lactate dehydrogenase 5: an old friend and a new hope in the war on cancer. Cancer Lett *358*, 1-7.

Billiard, J., Dennison, J.B., Briand, J., Annan, R.S., Chai, D., Colon, M., Dodson, C.S., Gilbert, S.A., Greshock, J., Jing, J.*, et al.* (2013). Quinoline 3-sulfonamides inhibit lactate dehydrogenase A and reverse aerobic glycolysis in cancer cells. Cancer Metab *1*, 19.

Birsoy, K., Wang, T., Chen, W.W., Freinkman, E., Abu-Remaileh, M., and Sabatini, D.M. (2015). An Essential Role of the Mitochondrial Electron Transport Chain in Cell Proliferation Is to Enable Aspartate Synthesis. Cell *162*, 540-551.

Carey, B.W., Finley, L.W., Cross, J.R., Allis, C.D., and Thompson, C.B. (2015). Intracellular alpha-ketoglutarate maintains the pluripotency of embryonic stem cells. Nature *518*, 413-416.

Carr, E.L., Kelman, A., Wu, G.S., Gopaul, R., Senkevitch, E., Aghvanyan, A., Turay, A.M., and Frauwirth, K.A. (2010). Glutamine uptake and metabolism are coordinately regulated by ERK/MAPK during T lymphocyte activation. J Immunol *185*, 1037-1044.

Cashen, A.F., Schiller, G.J., O'Donnell, M.R., and DiPersio, J.F. (2010). Multicenter, phase II study of decitabine for the first-line treatment of older patients with acute myeloid leukemia. J Clin Oncol *28*, 556-561.

Cerami, E., Gao, J., Dogrusoz, U., Gross, B.E., Sumer, S.O., Aksoy, B.A., Jacobsen, A., Byrne, C.J., Heuer, M.L., Larsson, E.*, et al.* (2012). The cBio cancer genomics portal: an open platform for exploring multidimensional cancer genomics data. Cancer Discov *2*, 401-404.

Dang, L., White, D.W., Gross, S., Bennett, B.D., Bittinger, M.A., Driggers, E.M., Fantin, V.R., Jang, H.G., Jin, S., Keenan, M.C.*, et al.* (2009). Cancer-associated IDH1 mutations produce 2-hydroxyglutarate. Nature *462*, 739-744.

Fazzari, M.J., and Greally, J.M. (2004). Epigenomics: beyond CpG islands. Nat Rev Genet *5*, 446-455.

Fendt, S.M., Bell, E.L., Keibler, M.A., Davidson, S.M., Wirth, G.J., Fiske, B., Mayers, J.R., Schwab, M., Bellinger, G., Csibi, A.*, et al.* (2013a). Metformin decreases glucose oxidation and increases the dependency of prostate cancer cells on reductive glutamine metabolism. Cancer Res *73*, 4429-4438.

Fendt, S.M., Bell, E.L., Keibler, M.A., Olenchock, B.A., Mayers, J.R., Wasylenko, T.M., Vokes, N.I., Guarente, L., Vander Heiden, M.G., and Stephanopoulos, G. (2013b). Reductive glutamine metabolism is a function of the alpha-ketoglutarate to citrate ratio in cells. Nat Commun *4*, 2236.

Figueroa, M.E., Abdel-Wahab, O., Lu, C., Ward, P.S., Patel, J., Shih, A., Li, Y., Bhagwat, N., Vasanthakumar, A., Fernandez, H.F.*, et al.* (2010). Leukemic IDH1 and IDH2 mutations result in a hypermethylation phenotype, disrupt TET2 function, and impair hematopoietic differentiation. Cancer Cell *18*, 553-567.

Frauwirth, K.A., Riley, J.L., Harris, M.H., Parry, R.V., Rathmell, J.C., Plas, D.R., Elstrom, R.L., June, C.H., and Thompson, C.B. (2002). The CD28 signaling pathway regulates glucose metabolism. Immunity *16*, 769-777.

Fukuda, H., Matsuzawa, T., Abe, Y., Endo, S., Yamada, K., Kubota, K., Hatazawa, J., Sato, T., Ito, M., Takahashi, T.*, et al.* (1982). Experimental study for cancer diagnosis with positron-labeled fluorinated glucose analogs: [18F]-2-fluoro-2-deoxy-D-mannose: a new tracer for cancer detection. Eur J Nucl Med *7*, 294-297.

Gao, J., Aksoy, B.A., Dogrusoz, U., Dresdner, G., Gross, B., Sumer, S.O., Sun, Y., Jacobsen, A., Sinha, R., Larsson, E.*, et al.* (2013). Integrative analysis of complex cancer genomics and clinical profiles using the cBioPortal. Sci Signal *6*, pl1.

Goldberg, E.B., and Colowick, S.P. (1965). The Role of Glycolysis in the Growth of Tumor Cells. 3. Lactic Dehydrogenase as the Site of Action of Oxamate on the Growth of Cultured Cells. J Biol Chem *240*, 2786-2790.

Hanse, E.A., Ruan, C., Kachman, M., Wang, D., Lowman, X.H., and Kelekar, A. (2017). Cytosolic malate dehydrogenase activity helps support glycolysis in actively proliferating cells and cancer. Oncogene.

Hirschhaeuser, F., Sattler, U.G., and Mueller-Klieser, W. (2011). Lactate: a metabolic key player in cancer. Cancer Res *71*, 6921-6925.

Karahoca, M., and Momparler, R.L. (2013). Pharmacokinetic and pharmacodynamic analysis of 5-aza-2'-deoxycytidine (decitabine) in the design of its dose-schedule for cancer therapy. Clin Epigenetics *5*, 3.

Kim, D.H., Sarbassov, D.D., Ali, S.M., King, J.E., Latek, R.R., Erdjument-Bromage, H., Tempst, P., and Sabatini, D.M. (2002). mTOR interacts with raptor to form a nutrient-sensitive complex that signals to the cell growth machinery. Cell *110*, 163-175.

Kim, J., Kundu, M., Viollet, B., and Guan, K.L. (2011). AMPK and mTOR regulate autophagy through direct phosphorylation of Ulk1. Nat Cell Biol *13*, 132-141.

Koivunen, P., Lee, S., Duncan, C.G., Lopez, G., Lu, G., Ramkissoon, S., Losman, J.A., Joensuu, P., Bergmann, U., Gross, S.*, et al.* (2012). Transformation by the (R)-enantiomer of 2-hydroxyglutarate linked to EGLN activation. Nature *483*, 484-488.

Koppenol, W.H., Bounds, P.L., and Dang, C.V. (2011). Otto Warburg's contributions to current concepts of cancer metabolism. Nat Rev Cancer *11*, 325-337.

Lamesch, P., Li, N., Milstein, S., Fan, C., Hao, T., Szabo, G., Hu, Z., Venkatesan, K., Bethel, G., Martin, P.*, et al.* (2007). hORFeome v3.1: a resource of human open reading frames representing over 10,000 human genes. Genomics *89*, 307-315.

Lee, S.M., Kim, J.H., Cho, E.J., and Youn, H.D. (2009). A nucleocytoplasmic malate dehydrogenase regulates p53 transcriptional activity in response to metabolic stress. Cell Death Differ *16*, 738-748.

Lewis, C.A., Parker, S.J., Fiske, B.P., McCloskey, D., Gui, D.Y., Green, C.R., Vokes, N.I., Feist, A.M., Vander Heiden, M.G., and Metallo, C.M. (2014). Tracing compartmentalized NADPH metabolism in the cytosol and mitochondria of mammalian cells. Mol Cell *55*, 253-263.

Liberti, M.V., and Locasale, J.W. (2016). The Warburg Effect: How Does it Benefit Cancer Cells? Trends Biochem Sci *41*, 211-218.

Lin-Moshier, Y., Sebastian, P.J., Higgins, L., Sampson, N.D., Hewitt, J.E., and Marchant, J.S. (2013). Re-evaluation of the role of calcium homeostasis endoplasmic reticulum protein (CHERP) in cellular calcium signaling. J Biol Chem *288*, 355-367.

Liu, P.P., Liao, J., Tang, Z.J., Wu, W.J., Yang, J., Zeng, Z.L., Hu, Y., Wang, P., Ju, H.Q., Xu, R.H.*, et al.* (2014). Metabolic regulation of cancer cell side population by glucose through activation of the Akt pathway. Cell Death Differ *21*, 124-135.

Locasale, J.W. (2013). Serine, glycine and one-carbon units: cancer metabolism in full circle. Nat Rev Cancer *13*, 572-583.

Lorenz, M.A., Burant, C.F., and Kennedy, R.T. (2011). Reducing time and increasing sensitivity in sample preparation for adherent mammalian cell metabolomics. Anal Chem *83*, 3406-3414.

Losman, J.A., Looper, R.E., Koivunen, P., Lee, S., Schneider, R.K., McMahon, C., Cowley, G.S., Root, D.E., Ebert, B.L., and Kaelin, W.G., Jr. (2013). (R)-2-hydroxyglutarate is sufficient to promote leukemogenesis and its effects are reversible. Science *339*, 1621-1625.

Lowman, X.H., McDonnell, M.A., Kosloske, A., Odumade, O.A., Jenness, C., Karim, C.B., Jemmerson, R., and Kelekar, A. (2010). The proapoptotic function of Noxa in human leukemia cells is regulated by the kinase Cdk5 and by glucose. Mol Cell *40*, 823-833.

Lu, C., Ward, P.S., Kapoor, G.S., Rohle, D., Turcan, S., Abdel-Wahab, O., Edwards, C.R., Khanin, R., Figueroa, M.E., Melnick, A.*, et al.* (2012). IDH mutation impairs histone demethylation and results in a block to cell differentiation. Nature *483*, 474-478.

Lum, J.J., Bui, T., Gruber, M., Gordan, J.D., DeBerardinis, R.J., Covello, K.L., Simon, M.C., and Thompson, C.B. (2007). The transcription factor HIF-1alpha plays a critical role in the growth factor-dependent regulation of both aerobic and anaerobic glycolysis. Genes Dev *21*, 1037-1049.

Lunt, S.Y., and Vander Heiden, M.G. (2011). Aerobic glycolysis: meeting the metabolic requirements of cell proliferation. Annu Rev Cell Dev Biol *27*, 441-464.

MacKenzie, E.D., Selak, M.A., Tennant, D.A., Payne, L.J., Crosby, S., Frederiksen, C.M., Watson, D.G., and Gottlieb, E. (2007). Cell-permeating alpha-ketoglutarate derivatives alleviate pseudohypoxia in succinate dehydrogenase-deficient cells. Mol Cell Biol *27*, 3282-3289.

Maddocks, O.D., Labuschagne, C.F., Adams, P.D., and Vousden, K.H. (2016). Serine Metabolism Supports the Methionine Cycle and DNA/RNA Methylation through De Novo ATP Synthesis in Cancer Cells. Mol Cell *61*, 210-221.

Mullen, A.R., Wheaton, W.W., Jin, E.S., Chen, P.H., Sullivan, L.B., Cheng, T., Yang, Y., Linehan, W.M., Chandel, N.S., and DeBerardinis, R.J. (2011). Reductive

carboxylation supports growth in tumour cells with defective mitochondria. Nature *481*, 385-388.

Parsons, D.W., Jones, S., Zhang, X., Lin, J.C., Leary, R.J., Angenendt, P., Mankoo, P., Carter, H., Siu, I.M., Gallia, G.L.*, et al.* (2008). An integrated genomic analysis of human glioblastoma multiforme. Science *321*, 1807-1812.

Pike Winer, L.S., and Wu, M. (2014). Rapid analysis of glycolytic and oxidative substrate flux of cancer cells in a microplate. PLoS One *9*, e109916.

Rani, R., and Kumar, V. (2016). Recent Update on Human Lactate Dehydrogenase Enzyme 5 (hLDH5) Inhibitors: A Promising Approach for Cancer Chemotherapy. J Med Chem *59*, 487-496.

Shilov, I.V., Seymour, S.L., Patel, A.A., Loboda, A., Tang, W.H., Keating, S.P., Hunter, C.L., Nuwaysir, L.M., and Schaeffer, D.A. (2007). The Paragon Algorithm, a next generation search engine that uses sequence temperature values and feature probabilities to identify peptides from tandem mass spectra. Mol Cell Proteomics *6*, 1638-1655.

Sonveaux, P., Copetti, T., De Saedeleer, C.J., Vegran, F., Verrax, J., Kennedy, K.M., Moon, E.J., Dhup, S., Danhier, P., Frerart, F.*, et al.* (2012). Targeting the lactate transporter MCT1 in endothelial cells inhibits lactate-induced HIF-1 activation and tumor angiogenesis. PLoS One *7*, e33418.

Sullivan, L.B., Gui, D.Y., Hosios, A.M., Bush, L.N., Freinkman, E., and Vander Heiden, M.G. (2015). Supporting Aspartate Biosynthesis Is an Essential Function of Respiration in Proliferating Cells. Cell *162*, 552-563.

Tahiliani, M., Koh, K.P., Shen, Y., Pastor, W.A., Bandukwala, H., Brudno, Y., Agarwal, S., Iyer, L.M., Liu, D.R., Aravind, L.*, et al.* (2009). Conversion of 5-methylcytosine to 5-hydroxymethylcytosine in mammalian DNA by MLL partner TET1. Science *324*, 930-935.

Tang, W.H., Shilov, I.V., and Seymour, S.L. (2008). Nonlinear fitting method for determining local false discovery rates from decoy database searches. J Proteome Res *7*, 3661-3667.

Tennant, D.A., and Gottlieb, E. (2010). HIF prolyl hydroxylase-3 mediates alpha-ketoglutarate-induced apoptosis and tumor suppression. J Mol Med (Berl) *88*, 839-849.

TeSlaa, T., Chaikovsky, A.C., Lipchina, I., Escobar, S.L., Hochedlinger, K., Huang, J., Graeber, T.G., Braas, D., and Teitell, M.A. (2016). alpha-Ketoglutarate Accelerates the Initial Differentiation of Primed Human Pluripotent Stem Cells. Cell Metab *24*, 485-493.

Tsukada, Y., Fang, J., Erdjument-Bromage, H., Warren, M.E., Borchers, C.H., Tempst, P., and Zhang, Y. (2006). Histone demethylation by a family of JmjC domain-containing proteins. Nature *439*, 811-816.

Turcan, S., Fabius, A.W., Borodovsky, A., Pedraza, A., Brennan, C., Huse, J., Viale, A., Riggins, G.J., and Chan, T.A. (2013). Efficient induction of differentiation and growth inhibition in IDH1 mutant glioma cells by the DNMT Inhibitor Decitabine. Oncotarget *4*, 1729-1736.

Tyanova, S., Temu, T., Sinitcyn, P., Carlson, A., Hein, M.Y., Geiger, T., Mann, M., and Cox, J. (2016). The Perseus computational platform for comprehensive analysis of (prote)omics data. Nat Methods *13*, 731-740.

Vander Heiden, M.G., Cantley, L.C., and Thompson, C.B. (2009). Understanding the Warburg effect: the metabolic requirements of cell proliferation. Science *324*, 1029-1033.

Vegran, F., Boidot, R., Michiels, C., Sonveaux, P., and Feron, O. (2011). Lactate influx through the endothelial cell monocarboxylate transporter MCT1 supports an NF-kappaB/IL-8 pathway that drives tumor angiogenesis. Cancer Res *71*, 2550-2560.

Wang, Y.P., Zhou, W., Wang, J., Huang, X., Zuo, Y., Wang, T.S., Gao, X., Xu, Y.Y., Zou, S.W., Liu, Y.B.*, et al.* (2016). Arginine Methylation of MDH1 by CARM1 Inhibits Glutamine Metabolism and Suppresses Pancreatic Cancer. Mol Cell *64*, 673-687.

Warburg, O., Wind, F., and Negelein, E. (1927). The Metabolism of Tumors in the Body. J Gen Physiol *8*, 519-530.

Wheaton, W.W., Weinberg, S.E., Hamanaka, R.B., Soberanes, S., Sullivan, L.B., Anso, E., Glasauer, A., Dufour, E., Mutlu, G.M., Budigner, G.S.*, et al.* (2014). Metformin inhibits mitochondrial complex I of cancer cells to reduce tumorigenesis. Elife *3*, e02242.

Wiese, S., Reidegeld, K.A., Meyer, H.E., and Warscheid, B. (2007). Protein labeling by iTRAQ: a new tool for quantitative mass spectrometry in proteome research. Proteomics *7*, 340-350.

Wise, D.R., DeBerardinis, R.J., Mancuso, A., Sayed, N., Zhang, X.Y., Pfeiffer, H.K., Nissim, I., Daikhin, E., Yudkoff, M., McMahon, S.B.*, et al.* (2008). Myc regulates a transcriptional program that stimulates mitochondrial glutaminolysis and leads to glutamine addiction. Proc Natl Acad Sci U S A *105*, 18782-18787.

Wise, D.R., Ward, P.S., Shay, J.E., Cross, J.R., Gruber, J.J., Sachdeva, U.M., Platt, J.M., DeMatteo, R.G., Simon, M.C., and Thompson, C.B. (2011). Hypoxia promotes isocitrate dehydrogenase-dependent carboxylation of alpha-ketoglutarate to citrate to support cell growth and viability. Proc Natl Acad Sci U S A *108*, 19611-19616.

Xie, H., Hanai, J., Ren, J.G., Kats, L., Burgess, K., Bhargava, P., Signoretti, S., Billiard, J., Duffy, K.J., Grant, A.*, et al.* (2014). Targeting lactate dehydrogenase--a inhibits tumorigenesis and tumor progression in mouse models of lung cancer and impacts tumor-initiating cells. Cell Metab *19*, 795-809.

Xu, W., Yang, H., Liu, Y., Yang, Y., Wang, P., Kim, S.H., Ito, S., Yang, C., Wang, P., Xiao, M.T.*, et al.* (2011). Oncometabolite 2-hydroxyglutarate is a competitive inhibitor of alpha-ketoglutarate-dependent dioxygenases. Cancer Cell *19*, 17-30.

Yang, Z., Savchenko, A., Yakunin, A., Zhang, R., Edwards, A., Arrowsmith, C., and Tong, L. (2003). Aspartate dehydrogenase, a novel enzyme identified from structural and functional studies of TM1643. J Biol Chem *278*, 8804-8808.

Yu, G., and He, Q.Y. (2016). ReactomePA: an R/Bioconductor package for reactome pathway analysis and visualization. Mol Biosyst *12*, 477-479.

Yuan, H.X., Xiong, Y., and Guan, K.L. (2013). Nutrient sensing, metabolism, and cell growth control. Mol Cell *49*, 379-387.

Zoncu, R., Efeyan, A., and Sabatini, D.M. (2011). mTOR: from growth signal integration to cancer, diabetes and ageing. Nat Rev Mol Cell Biol *12*, 21-35.